EarthN: A new Earth System Nitrogen Model

Benjamin W. Johnson[1,2] **Colin Goldblatt**[2]

[1]Department of Geological Sciences, University of Colorado, Boulder, Colorado, USA

[2]School of Earth and Ocean Sciences, University of Victoria, Victoria, British Columbia, Canada

Key Points:

- We model the evolution of nitrogen in all the reservoirs of Earth
- Total, non-core N and plate tectonics exert strong control on atmospheric mass
- Weathering and the Great Oxidation event cause atmospheric draw-down

Corresponding author: B. W. Johnson, benjamin.w.johnson@colorado.edu

Abstract

The amount of nitrogen in the atmosphere, oceans, crust, and mantle have important ramifications for Earth's biologic and geologic history. Despite this importance, the history and cycling of nitrogen in the Earth system is poorly constrained over time. For example, various models and proxies contrastingly support atmospheric mass stasis, net outgassing, or net ingassing over time. In addition, the amount available to and processing of nitrogen by organisms is intricately linked with and provides feedbacks on oxygen and nutrient cycles. To investigate the Earth system nitrogen cycle over geologic history, we have constructed a new nitrogen cycle model: EarthN. This model is driven by mantle cooling, links biologic nitrogen cycling to phosphate and oxygen, and incorporates geologic and biologic fluxes. Model output is consistent with large (2-4x) changes in atmospheric mass over time, typically indicating atmospheric drawdown and nitrogen sequestration into the mantle and continental crust. Critical controls on nitrogen distribution include mantle cooling history, weathering, and the total Bulk Silicate Earth+atmosphere nitrogen budget. Linking the nitrogen cycle to phosphorous and oxygen levels, instead of carbon as has been previously done, provides new and more dynamic insight into the history of nitrogen on the planet.

1 Introduction

Despite its importance and abundance in the Earth system, relatively little is known about the cycling of N throughout the major reservoirs of the Earth through time [*Zerkle and Mikhail*, 2017]. This is an important component of the Earth system, as the amount of N in the atmosphere can directly affect the climate [*Goldblatt et al.*, 2009; *Wordsworth and Pierrehumbert*, 2013] as well as biologic productivity [*Klingler et al.*, 1989]. Recent work has challenged the notion that N is primarily an atmospheric species, and instead the solid Earth may actually hold the majority of the planet's N budget [*Marty*, 2012; *Halliday*, 2013; *Johnson and Goldblatt*, 2015; *Barry and Hilton*, 2016; *Mallik et al.*, 2018].

While the major biologic and geologic fluxes affecting N distribution are known, their behavior over Earth history is not constrained. Early descriptions of atmospheric N_2 in the Precambrian admitted lack of data prevented speculation on what the atmospheric, and therefore mantle and continental crust, N content was at that time and how it has evolved since [*Delwiche*, 1977]. Subsequent work generally supports three hypotheses: steady-state atmospheric N mass over time [*Marty et al.*, 2013], net mantle outgassing over time [*Som et al.*, 2012, 2016], and net ingassing over time [*Nishizawa et al.*, 2007;

Goldblatt et al., 2009; *Johnson and Goldblatt*, 2015; *Barry and Hilton*, 2016; *Mallik et al.*, 2018; *Yoshioka et al.*, 2018]. Importantly, the assumption that atmospheric mass should be constant over Earth history is not an inherent property of the planet.

Preliminary modelling efforts considered sedimentary rocks as the main geologic storage and recycling vector for N [*Zhang and Zindler*, 1993; *Berner*, 2006] and compared N geochemically to the noble gases or carbon [*Tolstikhin and Marty*, 1998]. These studies found that there was little change ($< 1\%$) in atmospheric N_2 over at least the Phanerozoic [*Berner*, 2006] and possibly the majority of Earth history [*Zhang and Zindler*, 1993]. Additionally, while comparison to noble gases is valid for outgassing of oxidized magmas [*Libourel et al.*, 2003], this comparison is not valid at subduction boundaries, as N is mostly found as NH_4^+in subducted sediments [*Bebout and Fogel*, 1992] and oceanic crust [*Busigny et al.*, 2011].

The geologic treatment of N in previous models may have missed some important behavior. Specifically, only considering sedimentary rocks as a sink for biologically processed N [*Berner*, 2006] based on N/C ratios does not include hydrothermal addition of N to oceanic crust (Fig. 1), which is observed in modern and older altered crust [e.g., *Halama et al.*, 2014]. Sediment-only geologic N models also assume N and C behave similarly in subduction zones, which may not be true as N is likely found primarily as NH_4^+ geologically and C as organic C or CO_3^{2-}. In addition, previous whole-Earth modeling [*Tolstikhin and Marty*, 1998] maintained a steady-state upper mantle, in terms of N-isotopes and concentration, by recycling of sedimentary and sea-water-sourced N from the surface and N from the lower mantle entrained in plumes. This approach is incomplete, as, again, surface N is subducted to the mantle as NH_4^+ and it is likely that the mantle as a whole is not layered. Therefore, a mechanism of "re-filling" the upper mantle from the lower mantle slowly over time appears untenable.

Studies of several modern subduction zones suggest more dynamic N evolution, and that there is overall net transport of N into the solid Earth, either the mantle or arc-generated crust. Importantly, the N that survives the subduction barrier seems to mostly reside in the oceanic crust [*Li et al.*, 2007; *Mitchell et al.*, 2010]. There are many possible mineral hosts for such N, typically found as NH_4^+, during subduction, including NH_4^+-bearing feldspars, pyroxenes, beryls, and phlogopite in the mantle [*Watenphul et al.*, 2009, 2010; *Bebout et al.*, 2015] . Such crystalline N in altered crust appears to be more likely

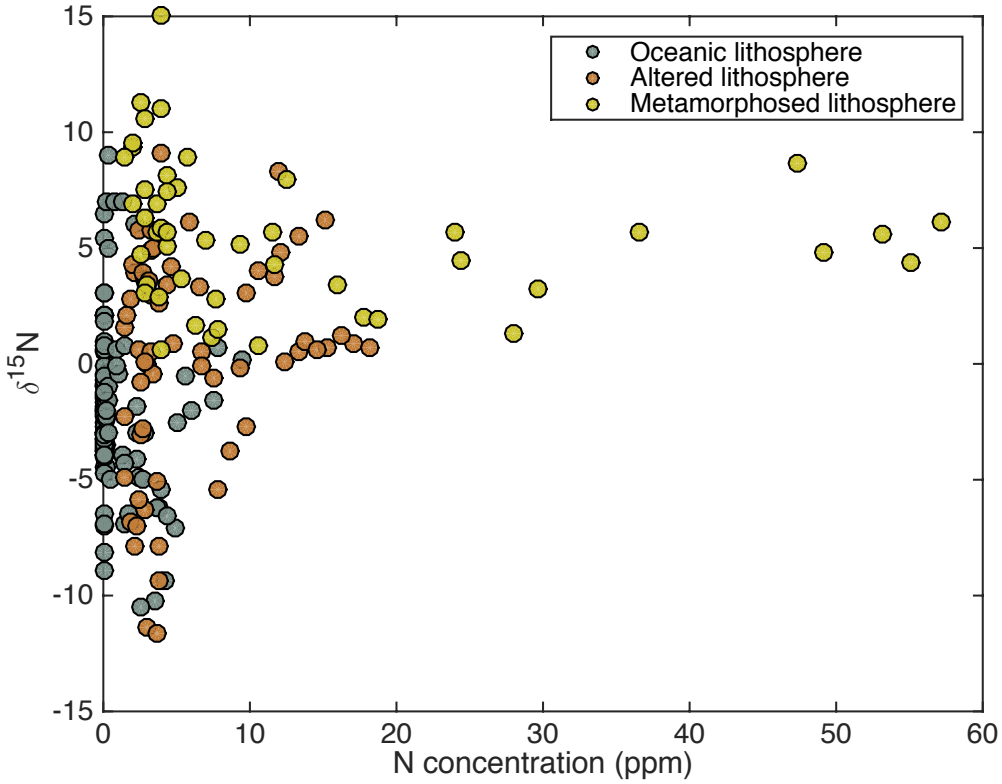

Figure 1: δ^{15}N plotted against N concentration (ppm) for oceanic lithosphere. Data are from the compilation of *Johnson and Goldblatt* [2015]. Shown are values from fresh lithosphere, altered lithosphere, and metamorphosed. Altered lithosphere has experienced temperatures of <300 °C and metamorphosed samples have experienced temperatures >300 °C. As oceanic lithosphere experiences alteration, N concentration increases, and initially depleted δ^{15}N values, with a mean of -1.8‰ are enriched, indicating additional N is sourced from biologic material, which has δ^{15}N of 5‰. Altered lithosphere rocks include MORBs while metamorphosed lithosphere rocks include blueschists, eclogites, and metagabbros.

to be carried into the mantle, whereas sedimentary N tends to return to the atmosphere at subduction zones [*Fischer et al.*, 2002; *Elkins et al.*, 2006; *Halama et al.*, 2014].

As such, we are presented with a conundrum. Modeling efforts suggest that the atmosphere and solid Earth have remained in equilibrium in terms of N-content over time. Contrastingly, geochemical evidence suggests there may be net transport of N from the surface to the mantle over time. It is from this conundrum that the construction of an Earth-system N cycle model, EarthN, follows.

Previous Earth system models implicitly have biologic processing [e.g., *Stüeken et al.*, 2016], but none so far actually explicitly model the behavior of organisms. Biologic productivity and activity is the gate-keeper between the atmosphere and the solid Earth. Similarly, recent work has modeled the nitrogen cycle but without biology [*Laneuville et al.*, 2018], to serve as a background for interpretations and models including biology. Nitrogen can cycle throughout the atmosphere, biosphere, sedimentary rocks, and crystalline Earth, thus constructing a model that integrates both biologic and geologic fluxes is critical for investigating the N-cycle over Earth history.

2 Model setup

The model is divided into a number of boxes. These are the atmosphere, three shallow ocean boxes (low-latitude, high-latitude, shelf), deep ocean, two biologically active sediment boxes (reactive shelf, reactive deep), sediments not in communication with the ocean (shelf, deep), and geologic reservoirs (mantle, oceanic crust, continental crust).

The model contains N as N_2, NO_3^-, and NH_4^+, the last of which can be in the ocean or in geologic reservoirs. We also include other biologically relevant species: PO_4^{3-} and O_2, as well as inorganic tracers: K,^{40}K,^{40}Ar, and^{36}Ar. Phosphate directly affects biologic productivity and O_2 affects both productivity and which pathways of the biologic N cycle are in operation. Nitrogen is geochemically similar to K when found as $NH_4^+$and geochemically similar to Ar when found as N_2. As K and Ar are not biologically important elements, they serve as both a calibration and validation of the purely physical aspects of the model (Appendix C:).

Biogeochemical fluxes are after *Fennel et al.* [2005], with a number of updates. Most geologic fluxes are driven by mantle cooling history after *Korenaga* [2010] and *Padhi et al.* [2012], which produces estimates of mantle temperature, crust production, and

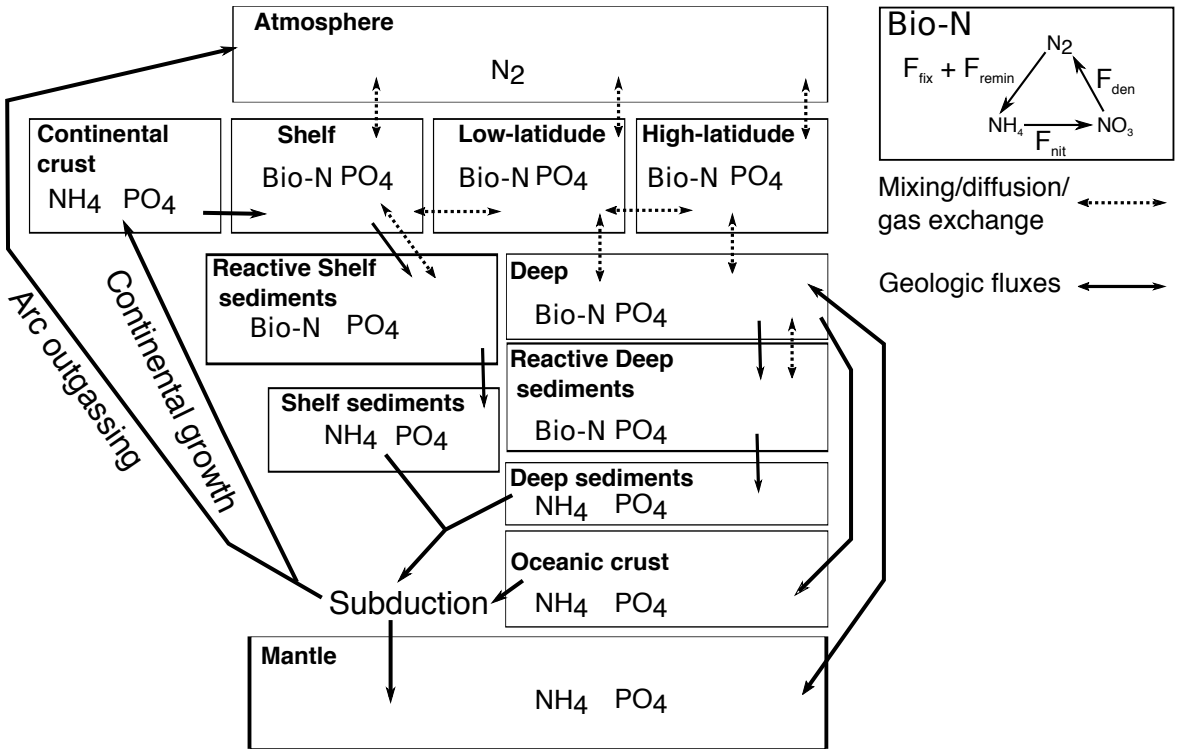

Figure 2: Earth system nitrogen cycle model schematic. In addition, we included K, ^{40}K, ^{40}Ar, ^{36}Ar, and ^{40}Ca as checks on non-biologic cycles, though these are not shown here.

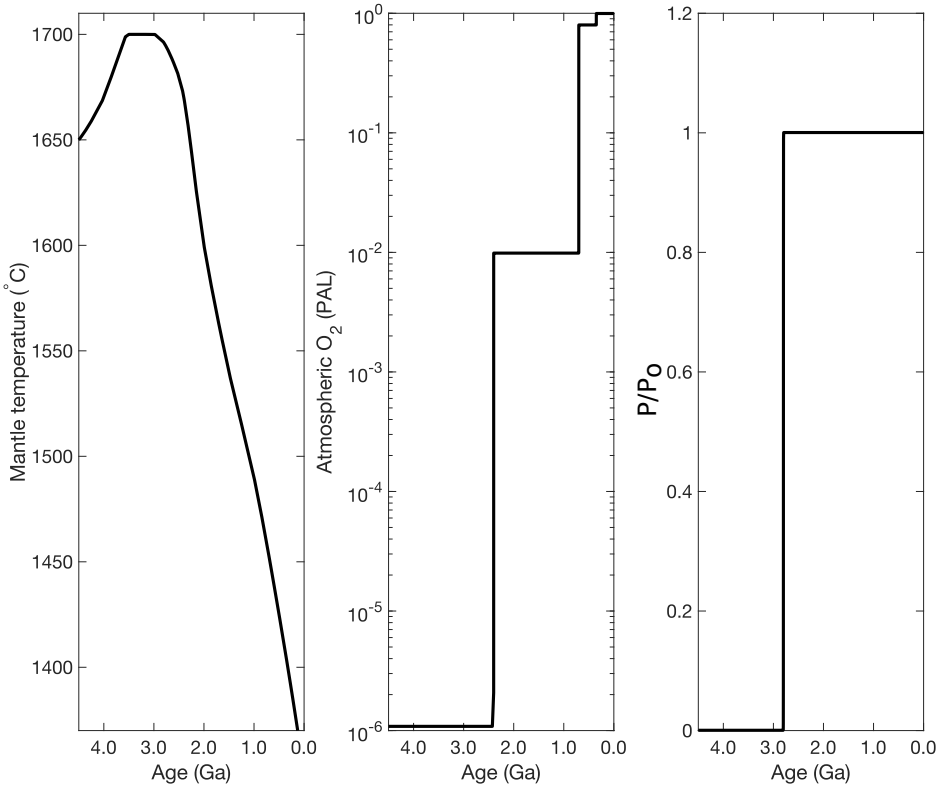

Figure 3: Model forcings, including average mantle potential temperature (°C) [*Korenaga*, 2010], atmospheric O_2 [e.g., *Lyons et al.*, 2014], and primary productivity (P) compared to modern (P_o) constant [*Goldblatt et al.*, 2006].

spreading rate through time (Fig. 3). Some runs have a constant proportion of subducted material retained to the mantle, and some link subducted fraction to mantle temperature.

The following is first a brief description of element cycles, then a detailed description of the model setup. We discuss each model box, the species contained within said box, and the fluxes that affect the amount of each species in the box. We use R_j^i to represent reservoir in moles size of species j in box i and C_j^i to represent the corresponding concentration. F_k^i represents fluxes of type k in box i (Table 1). There are a number of fluxes that are sensitive to reactant concentration (e.g., Michaelis-Menten behavior), and are shown as v_l where l is specific to each sensitivity v. Parameter values are given in Table 2 and full differential equations are given in Appendix B.

2.1 Brief element cycle descriptions

The model Earth-system N cycle is as follows. Atmospheric N_2 dissolves in the ocean, where it can be fixed (i.e., breaking the N triple bond) by bacteria. Fixed N then cycles biologically, and is released as waste or when organisms die. In oxygenated water, this reduced biologic N is quickly nitrified (NH_4^+ to NO_3^-) by bacteria; in anoxic water it remains as NH_4^+. Some organic material sinks into the deep ocean, where most gets remineralized into either NH_4^+or NO_3^- depending on O_2 levels, and a small portion sinks to the sediments. In the sediments, organic matter breaks down and bonds as NH_4^+ into clays and other K-bearing minerals. Some N also gets incorporated into oceanic crust during hydrothermal alteration. Sediments and oceanic crust get subducted, with a portion of N going into the mantle, a portion outgassed to the atmosphere, and a portion incorporated into arc-generated crust. Mantle N can be outgassed at mid-ocean ridges. Continental crust N, organic or inorganic, can be weathered and added back to the ocean.

Phosphate enters the ocean due to continental weathering and from mid-ocean ridge outgassing. In the shallow ocean, it is consumed during primary production, both that based on already fixed N and that based on fixing new N. It is then exported to the deep or lower shelf ocean, where it is either remineralized or buried in sediments. Sedimentary and altered oceanic crust PO_4^{3-} can be subducted. A portion goes into the mantle, and a portion into the continental crust.

The model cycles for K and Ar are only affected by physical, non-biologic processing. All isotopes of both elements mix between ocean boxes, and^{40}K decays to^{40}Ar in

every box where it is found. Continental weathering releases K to the shelf ocean, and Ar to the atmosphere. Air sea gas exchange moves Ar from the surface ocean boxes to the atmosphere. Both species can get incorporated into oceanic crust during hydrothermal alteration, and K can be incorporated into sediments. Again, during subduction, some K and Ar is transported to the mantle, and the remainder either goes to the continental crust (K) or the atmosphere (Ar). Both are added to the deep ocean during mid-ocean ridge outgassing.

2.2 ^{40}K-decay

Radioactive decay of ^{40}K produces ^{40}Ar in all boxes where ^{40}K is present:

$$F^i_{\mathrm{rd}} = \lambda X_{40\mathrm{K}} R^i_{40\mathrm{K}} \tag{1}$$

for i ={all ocean and geologic boxes} where $X_{40\mathrm{K}}$ is the proportion of decays that form ^{40}Ar and λ is the decay constant of ^{40}K.

2.3 Atmosphere

The atmosphere contains N_2, O_2, and both isotopes of Ar. N_2, ^{40}Ar, and ^{36}Ar exchange with the ocean following stagnant-lid gas exchange [*Liss and Slater*, 1974], with fluxes positive in the direction of sea to air:

$$F^i_{\mathrm{as}} = u_{\mathrm{l},j} A^i \left(C^i_j - H_j P_j \right) \tag{2}$$

for boxes i = {low, high, shelf} oceans and species j = {N_2, ^{40}Ar, ^{36}Ar, O_2}. $u_{\mathrm{l},j}$ is piston velocity in m yr^{-1} calculated by dividing the diffusion constant (D_i) by thickness of stagnant boundary (z_{film}); A^i is ocean box surface area (m^2); C^j_i is concentration of species j in box i; H^j is Henry's law constant for species j (mol L^{-1} atm^{-1}); and P^j is partial pressure of gas j, calculated as:

$$P_j = \frac{R^{\mathrm{atm}}_j}{n_{\mathrm{a}}} \tag{3}$$

where n_{a} is the number of moles corresponding to one atmosphere pressure (Table 2).

Gasses are also added to the atmosphere via outgassing at arcs and both isotopes of Ar are added from continental crust weathering (Sec. 2.5).

Table 1: Full list of fluxes used in model. Shown are flux symbol, brief description, and which model species are affected by each flux. In ocean boxes (low, high, shelf, deep), all species includes NO_3^- and NH_4^+, while in geologic boxes, all species just includes moles of N.

Flux	**Description**	**Species affected**
F_{rd}	radioactive decay	^{40}Ar, ^{40}K
F_{as}	air-sea gas exchange	^{40}Ar, ^{36}Ar, N_2
F_{mix}	water-mixing	all species
F_{nit}	nitrification	NO_3^-, NH_4^+
F_{denit}	denitrification	NO_3^-, N_2
F_{oldN}	production from fixed N	NO_3^-, NH_4^+, PO_4^{3-}
F_{newN}	production from newly fixed N	N_2, PO_4^{3-}
F_{out}	export from shallow ocean boxes	NO_3^-, NH_4^+, N_2, PO_4^{3-}
F_{remin}	remineralization in shelf and deep	NO_3^-, NH_4^+, PO_4^{3-}
F_{bur}	burial in sediments	N, PO_4^{3-}
F_{seddif}	diffusion into sediments, out of water	NH_4^+
F_{sub}	subduction of crust and sediments	all species
F_{subT}	total subduction	all species
F_{subnet}	net subduction	all species
F_{hydro}	hydrothermal alteration	all species
F_{w}	weathering	all species
F_{cg}	continental growth	all species
F_{scg}	continental growth from shelf sediments	all species
F_{ogarc}	outgassing-arcs	all species
F_{ogmor}	outgassing-mid ocean ridge	all species

Oxygen levels are prescribed. Levels start at 10^{-6} present atmospheric level (PAL = 2×10^{19} mol) through the Hadean and Archean. . Atmospheric O_2 increases to 0.01 PAL over 100 Myr at 2.4 Ga, then to 0.8 PAL at 0.630 Ga (beginning of the Ediacaran). Oxygen rises to modern levels at 0.418 Ga (Devonian). Surface ocean O_2 concentrations are calculated assuming a Henry's law equilibrium.

2.4 Ocean

The ocean is divided into four boxes: high- and low-latitude shallow ocean, shelf ocean, and deep ocean. All species in the model exist in the ocean. There are a number of fluxes, both physical and biogeochemical that occur. Some can occur in all boxes, and some only in specific boxes. Broadly, primary production occurs in shallow ocean boxes, remineralization and burial occur in deep and shelf boxes, and nitrification and denitrification occur in all boxes.

2.4.1 All boxes

There is physical water mixing between all ocean boxes. Mixing out of an ocean box is simply the product of concentration of species j in box i and the sum of the water fluxes (Δ^{i-i*}, in L yr^{-1}) between box i and all other boxes ($i*$). Mixing in to box i is the sum of the product of the concentrations of species j in each other box ($i*$) and the water flux between box i and each other box (Δ^{i-i*}):

$$F^{i}_{\mathrm{mix},j} = -C^{i}_{j} \sum_{i*} \Delta^{i-i*} + \sum_{i*} C^{i*}_{j} \Delta^{i-i*} \tag{4}$$

If, for example, i ={low}, then $i*$ ={high, shelf, deep}, and Δ^{i-i*} is mixing between low and high, low and shelf, and low and deep boxes.

Nitrification occurs in all boxes. The rate of nitrification is dependent on O_2 and NH_4^+concentrations:

$$v^{i}_{\mathrm{Onit}} = \frac{C^{i}_{\mathrm{O2}}}{C^{i}_{\mathrm{O2}} + K_{\mathrm{Oni}}} \tag{5}$$

$$v^{i}_{\mathrm{NOnit}} = \frac{C^{i}_{\mathrm{NH4}}}{C^{i}_{\mathrm{NH4}} + K_{\mathrm{Nni}}} \tag{6}$$

The full equation can be parameterized as:

$$F^i_{\mathrm{nit}} = \mu_{\mathrm{NH4}} v^i_{\mathrm{Onit}} v^i_{\mathrm{NHnit}} R^i_{\mathrm{NH4}} \tag{7}$$

for box i ={low, high, shelf, deep}, and where K_{Oni} is the half-saturation uptake concentration of O_2 used in nitrification (20 μM), K_{Nni} is half-saturation uptake concentration of O_2 used in nitrification (100 μM), and μ_{NH4} is a rate constant (yr $^{-1}$).

Denitrification can also occur in every ocean box (i ={low, high, shelf, deep}). It has been observed to follow first-order rate kinetics, with a half-saturation NO_3^- concentration (K_{d}) of 8 μM [*Goering*, 1985; *Evrard et al.*, 2013]:

$$v^i_{\mathrm{NOde}} = \frac{C^i_{\mathrm{NO3}}}{C^i_{\mathrm{NO3}} + K_{\mathrm{d}}} \tag{8}$$

In contrast to nitrification, denitrification only occurs at low O_2 levels [*Crowe et al.*, 2012; *Dalsgaard et al.*, 2014], herein parameterized as a Michaelis-Menten type reaction:

$$v^i_{\mathrm{Ode}} = \frac{C^i_{\mathrm{O2}}}{C^i_{\mathrm{O2}} + O_{\mathrm{inhib}}} \tag{9}$$

where O_{inhib} is 205 nM [*Dalsgaard et al.*, 2014]. Thus, we parameterize denitrification as:

$$F^i_{\mathrm{den}} = (1 - v^i_{\mathrm{Ode}}) v^i_{\mathrm{NOde}} R^i_{\mathrm{NO3}} \tag{10}$$

2.4.2 Shallow ocean

Primary production occurs in all shallow ocean boxes (i ={low, high, shelf}). There are two types of productivity [*Fennel et al.*, 2005]: that based on already fixed N (F_{oldN}) and that based on newly-fixed N_2 (F_{newN}). These two fluxes together equal total export production (F^i_{ExT}). The proportion of F_{oldN} to F_{newN} depends, in part, on the N:P ratio, which we assume will always move towards Redfield (i.e., 16:1). We parameterize this relationship as:

$$L^i_{\mathrm{R}} = \frac{N/P^i}{N/P^i + K_{\mathrm{NP}}} \tag{11}$$

where K_{NP} is 8.

In addition, F_{oldN} can be PO_4^{3-} or N-limited:

$$L_{\mathrm{N}}^{i} = \frac{N_{\mathrm{all}}^{i}}{N_{\mathrm{all}}^{i} + K_{\mathrm{N}}} \tag{12}$$

$$L_{\mathrm{P}}^{i} = \frac{C_{\mathrm{PO4}}^{i}}{C_{\mathrm{PO4}}^{i} + K_{\mathrm{P}}} \tag{13}$$

where K_{N} and K_{P} are the half saturation uptake values for N and PO_4^{3-}. N_{all}^{i} is the sum of C_{NH4}^{i} and C_{NO3}^{i} in box i. We also assume productivity (P) was 1000 times less efficient before the evolution of oxygenic photosynthesis:

$$\frac{P}{P_o} = ((1 + 1 \times 10^{-3}) + \tanh((t - \mathrm{Phot_{On}})/0.1)) \times 0.5; \tag{14}$$

where P_o is modern primary productivity efficiency (1) and $\mathrm{Phot_{On}}$ is the age of oxygenic photosynthesis evolution.

Thus, F_{oldN}^{i} is:

$$F_{\mathrm{oldN}}^{i} = \frac{P}{P_o} L_{\mathrm{R}}^{i} L_{\mathrm{N}}^{i} L_{\mathrm{P}}^{i} R_{\mathrm{PO4}}^{i} / \tau_{\mathrm{prod}} \tag{15}$$

for boxes i ={low, high, shelf} and where τ_{prod} is a production timescale, set to 0.5 yr.

Production from N_2 fixing is PO_4^{3-}-limited, but also depends on N-concentrations and partial pressure of N_2. There is a Michaelis-Menten relationship to partial pressure [*Klingler et al.*, 1989]:

$$v_{\mathrm{fix}} = \frac{R_{\mathrm{N2}}^{\mathrm{atm}}}{R_{\mathrm{N2}}^{\mathrm{atm}} + K_{\mathrm{f}}}; \tag{16}$$

where K_{f} is 9.87×10^{18} moles, or about the equivalent of 50 mbar pressure.

Thus, total production based on newly-fixed N_2 is:

$$F_{\mathrm{newN}}^{i} = \frac{P}{P_o}(1 - L_{\mathrm{R}}^{i}) L_{\mathrm{P}}^{i} v_{\mathrm{fix}} R_{\mathrm{PO}}^{i} / \tau_{\mathrm{prod}} \tag{17}$$

We note that we do not include abiotic N-fixing in our model [e.g., *Navarro-González et al.*, 2001]. Total export production (F_{ExT}^{i}) from boxes i ={low, high, shelf} is the sum of F_{oldN}^{i} and F_{newN}^{i}. Export production in both the low- and high-latitude boxes go to the

deep ocean, and shelf export stays in the shelf box. Phosphate loss ($F^i_{\text{out,PO4}}$) from shallow boxes is equal to F^i_{ExT}. Fixed NO_3^- and NH_4^+losses are equal to:

$$F^i_{\text{out},j} = 16F^i_{\text{oldN}}\frac{C^i_j}{N^i_{\text{all}}} \tag{18}$$

for $j = \{NO_3^-, NH_4^+\}$ and N_2 loss is:

$$F^i_{\text{out,N2}} = 16F^i_{\text{newN}} \tag{19}$$

as we keep track of moles N, not moles N_2.

2.4.3 Shelf ocean, deep ocean, reactive shelf and deep sediments

PO_4^{3-} and N can be remineralized or buried, and K can be buried in sediments. The efficiency of remineralization depends on oxygen concentration:

$$f^i_{\text{aerobic}} = \frac{C^i_{\text{O2}}}{C^i_{\text{O2}} + K_{\text{O}}} \tag{20}$$

$$F^i_{\text{reminfrac, j}} = 0.9f^i_{\text{aerobic}} + 0.7(1 - f^i_{\text{aerobic}}). \tag{21}$$

for boxes $i = \{$shelf ocean, deep ocean, reactive shelf sediments, reactive deep sediments$\}$ and species $j = \{PO_4^{3-}, NH_4^+\}$ and where K_{O} is 50 μM. The values in the above equations are tuned to have aerobic remineralization convert 90% of export production, while only 70% gets remineralized under anaerobic conditions. Nitrogen remineralization and burial is assumed to be in Redfield ratio (i.e.,16:1) compared to PO_4^{3-}. Nitrogen is remineralized as NH_4^+.

Export production from the high and low-latitude shallow boxes is remineralized in the deep ocean and export production in the shelf ocean is remineralized in the shelf ocean. That which is not remineralized in the deep or shelf ocean boxes goes to the reactive deep and shelf sediments, respectively. Remineralization can occur in these reactive sediment boxes, with anything not remineralized buried to the non-reactive deep and shelf sediments. Additionally, nitrification, denitrification, and diffusion occur in the reactive sediment layers. Diffusion (F^i_{diff}) is parameterized as:

$$F^i_{\text{diff},j} = D_j\left(C^{i*}_{\text{O2},j} - \frac{C^i_{\text{O2},j}}{D_{\text{length}}}\right)SA^{i*} \tag{22}$$

for boxes i = {Reactive shelf sediments, reactive deep sediments} and $i*$ = {shelf ocean, deep ocean}. D_j is the diffusion constant and D_{length} is diffusive length, which is set to 0.01 m.

Table 2: All model constants, shown with references. References are: H14 [*Haynes et al.*, 2014], S99 [*Sander*, 1999], F05 [*Fennel et al.*, 2005], LS74 [*Liss and Slater*, 1974], B16 [*Bristow et al.*, 2016], D14 [*Dalsgaard et al.*, 2014], G85 [*Goering*, 1985], E13 [*Evrard et al.*, 2013], K89 [*Klingler et al.*, 1989], JG15 [*Johnson and Goldblatt*, 2015], W10 [*Winter*, 2001], and K10 [*Korenaga*, 2010]

Parameter	**Definition**	**Value**	**Reference**
λ	decay constant of^{40}K (yr $^{-1}$)	5.543×10^{-10} yr $^{-1}$	H14
X_{40}	fraction of decay producing ^{40}Ar	0.1072	H14
D_{N_2}	Diffusion constants (cm^2 s^{-1})	1.88×10^{-5}	H14
D_{Ar}		1.88×10^{-5}	H14
D_{O_2}		2.5×10^{-5}	H14
D_{length}	Diffusion length	0.01 m	
H_{N_2}	Henry's law constants (mol L^{-1} atm $^{-1}$)	1.3×10^{-3}	S99
H_{Ar}		6.1×10^{-4}	S99
H_{O_2}		6.1×10^{-4}	S99
n_a	moles equal to one atm pressure	1.72×10^{20}	this study
d	ocean depth (m)	4500	F05
z_{film}	stagnant lid thickness (m)	1.5×10^{-5}	LS74
A^{high}	ocean box surface area (m^2)	2.3×10^{12}	F05
A^{low}		2.3×10^{12}	F05
A^{shelf}		5.1×10^{11}	F05
V^{high}	ocean box volumes (L)	9×10^{18}	F05
V^{low}		9×10^{18}	F05
V^{shelf}		1.5×10^{18}	F05
V^{deep}		8.1×10^{20}	F05
$\Delta^{\text{low-high}}$	mixing between ocean boxes (Sv)	30	F05
$\Delta^{\text{low-shelf}}$		30	F05
$\Delta^{\text{low-deep}}$		30	F05
$\Delta^{\text{high-shelf}}$		30	F05

Continued on next page

Table 2 Model Constants – continued from previous page

Parameter	Definition	Value	Reference
$\Delta^{\text{high-deep}}$		50	F05
$\Delta^{\text{shelf-deep}}$		5-100	This study
K_{Oni}	half-saturation uptake of O_2 in nitrification	283 nM	B16
K_{Nni}	half-saturation uptake of NH_4^+in nitrification	100 μM	F05
K_{d}	half-saturation uptake of NO_3^- in denitrification	8 μM	
K_{NP}	Redfield term	8.47 μM	G85, E13
K_{N}	half-saturation uptake of total N	1.6 μM	F05
K_{P}	half-saturation uptake of PO_4^{3-}	0.1 μM	F05
K_{f}	half-saturation uptake of N_2 during fixing	9.87×10^{18} mol	K89
K_{O}	O_2 concentration term	50 μM	
K_{dist}	percent of species extracted during MORB-genesis	0.90	
τ_{prod}	Export production time-scale	0.5 yr^{-1}	
τ_{W}	rate constant of weathering	3.33×10^{-9} yr^{-1}	
τ_{scg}	rate constant of	1×10^{-8} yr^{-1}	this study
μ_{NH4i}	nitrification rate constant	1 yr^{-1}	F05
O_{inhib}	Oxygen inhibition for denitrification	205 nM	D14
u_{co}	Modern spreading rate	0.05 m yr^{-1}	K10
T_o	Modern mantle potential temperature	1350 °C	K10
ρ_c	Ocean crust density	3000 kg m^{-3}	
M^{desed}	mass of deep sediments	7.3×10^{23} g	JG15
M^{occrust}	mass of ocean crust	5.4×10^{24} g	JG15
M^{mantle}	mass of mantle	4×10^{27} g	JG15
	shelf sediments to cont. crust		
a_{W}	Anoxic weathering fraction	0.1	this study
k_{weath}	Weathering rate O_2 dependence	1×10^{-3}	this study
V_{hydro}	hydrothermal circulation volume	1.6 Sv	this study
Heff	Hydrothermal retention efficiency	0.1-1, varies by species	this study
P_m	percent partial melt during MORB-genesis	10%	W01

Continued on next page

Table 2 Model Constants – continued from previous page

Parameter	Definition	Value	Reference
S	spreading rate (m yr^{-1})	varies	K10
h_{sed}	sediment thickness	500 m	this study
h_c	Ocean crust thickness	16000 to 8000 m	K10
L_s	length of subduction zones	4×10^7 m	this study
L_r	length of mid-ocean ridges	8×10^7 m	this study
f_{shsed}	fraction shelf sediments subducted	1×10^{-9}	this study
f_{Ncgarc}	fraction N added to continental crust	0.5	this study

2.5 Geologic model

The model is driven by a mantle cooling history from *Korenaga* [2010] and *Padhi et al.* [2012]. This model suggests that mantle temperatures (T_m) increased through the early Archean, reached their peak in the middle Archean, and have been decreasing to the modern day (Table 3, Fig. 3). Heat flux (Q) followed a distinct evolution, reaching its maximum later than the mantle temperature apex (Table 3). Temperature and heat flux are used to parameterize a plate velocity (u_c):

$$u_c = u_{co} \frac{Q}{Qo} \left(\frac{T_o}{T_m} \right)^2 \tag{23}$$

where u_{co}, Q_o, and T_o are modern plate velocity (0.05 m yr^{-1}), heat flux (39 TW), and average mantle temperature (1350 °C).

The model then calculates crust production at mid-ocean ridges by combining spreading rate with ridge length (L_r, m) and crust thickness (h_c, m):

$$O_p = u_c h_c L_r \rho_c \tag{24}$$

where ρ_c is crust density (kg m^{-3}), and h_c decreases linearly through time [*Sleep and Windley*, 1982] from 16 km at the beginning of the model to 8 km at $t = 4.5$ Gyr. We assume that the amount of crust subducted (O_s) is equal to O_p.

Table 3: Mantle temperature (T_m) history, heat flux (Q), and spreading rate (u_c) evolution from *Korenaga* [2010]; *Padhi et al.* [2012].

Age (Ga)	T_m **°C**	Q **(TW)**	u_c **(cm yr^{-1})**
0	1350	39	5.00
0.5	1425	43	5.55
1.0	1490	41	4.68
1.5	1540	40	4.22
2.0	1600	39	3.75
2.5	1680	38	3.28
3.0	1700	37	3.05
3.5	1700	37	3.05
4.0	1670	37.5	3.23
4.5	1650	38	3.38

2.6 Sediments

Anything that does not get remineralized in the reactive sediment boxes gets buried (F^i_{bur}) in sediments:

$$F^i_{\text{bur}} = F^{i*}_{\text{burial}} - F^{i*}_{\text{remin}} \tag{25}$$

for boxes i = {shelf sediments, deep sediments} and $i*$ = {reactive shelf sediments, reactive deep sediments}.

Species are subducted from both deep and shelf sediments. A constant fraction of shelf sediment species gets subducted,:

$$F^{\text{shsed}}_{\text{sub,j}} = f_{\text{shsed}} R^{\text{shsed}}_j \tag{26}$$

where f_{shsed} is the fraction of shelf sediments that subduct (1×10^{-9} yr^{-1}). Deep sediments subducted are equal to:

$$F^{\mathrm{dsed}}_{\mathrm{sub,j}} = \frac{m^{\mathrm{dsed}}_{\mathrm{sub}} R^{\mathrm{dsed}}_{j}}{M^{\mathrm{dsed}}} \tag{27}$$

where m^{desed} is the mass of deep sediments subducted and M^{dsed} is the mass of deep sediments (7.4×10^{23} g). Mass of sediments subducted is:

$$m^{\mathrm{dsed}}_{\mathrm{sub}} = L_{\mathrm{s}} S h_{\mathrm{sed}} \rho_{\mathrm{sed}} \tag{28}$$

where L_s is subduction zone length (m), S is spreading rate (m yr^{-1}) calculated from Korenaga model, h_{sed} is thickness of sediments (500 m), and ρ_{sed} is sediment density (2.5 g cm^{-3}).

In addition, shelf sediments have a residence time of 100 Myr, or a rate constant of $\tau_{\mathrm{scg}} = 1\times10^{-8}$ yr^{-1}. Shelf sediments are added to the continental crust, representing a proxy for continental growth by collision and accretion:

$$F_{\mathrm{scg,j}} = \tau_{\mathrm{scg}} R^{\mathrm{shsed}}_{j} \tag{29}$$

for j ={all species}.

2.7 Crust

2.7.1 Oceanic

Species can enter the oceanic crust through hydrothermal alteration, and the leave the oceanic crust during subduction. We envision hydrothermal processes essentially as serpentinization, and overall it adds N to the oceanic lithosphere [*Halama et al.*, 2014]. The amount of hydrothermal alteration is related to both speciation and a volume of hydrothermal fluid flow per year:

$$F_{\mathrm{hydro,\,j}} = C^{\mathrm{deep}}_{j} V_{\mathrm{hydro}} H_{\mathrm{eff}} \tag{30}$$

for all model species. H_{eff} is 1 for K and NH_4^+, 0.5 for NO_3^- and PO_4^{3-}, and 0.01 for Ar. We set V_{hydro} equal to 1.6 Sv [*Elderfield and Schultz*, 1996; *German and Seyfried*, 2014] for nominal runs, but allowed it to vary during sensitivity tests.

The subduction flux is calculated by multiplying the mass of crust subducted per year by each species concentration in the crust:

$$F^{\mathrm{oc}}_{\mathrm{sub},j} = \frac{R^{\mathrm{ocrust}}_{j} O_p}{M^{\mathrm{occrust}}} \tag{31}$$

where O_p is ocean crust produced and M_{occrust} is the total mass of crust (g).

Thus, the total amount of each species subducted (F_{subT}) is

$$F_{\mathrm{subT},j} = F^{\mathrm{oc}}_{\mathrm{sub},j} + F^{\mathrm{dsed}}_{\mathrm{sub},j} + F^{\mathrm{shsed}}_{\mathrm{sub},j} \tag{32}$$

Subducted species will either be driven off the slab and sediments or carried beyond the subduction barrier and into the mantle. The proportion that is driven off the slab is determined by mantle temperature: higher temperature means less material goes into the mantle, and lower temperature means more material goes into the mantle. Subducted fraction is calculated from an average geothermal gradient (G_{sub} in °C km^{-1}), which in turn is calculated from an average mantle temperature (T_m):

$$G_{\mathrm{sub}} = \frac{12.2(T_m - 273)}{2900} \tag{33}$$

where T_m is in kelvin, 2900 is mantle depth in km, and 12.2 is a conversion factor to adjust average mantle temperature, consistent with the modern average mantle geothermal gradient. Subducted fraction is a hyperbolic tangent fit to the data from modern geothermal gradients and subducted fluxes at three modern subduction zones [*Elkins et al.*, 2006; *Mitchell et al.*, 2010; *Zelenski et al.*, 2012], and can vary between 0.1 and 1:

$$f_{\mathrm{sub}} = 0.5\left(1.1 - 0.9\tanh\left(\frac{G_{\mathrm{sub}} - 6}{0.6}\right)\right) \tag{34}$$

The values inside the tanh parenthetical, 6 and 0.6, have units of °C km^{-1}. We again note previous work that has indicated there is likely more complication in the ratio between N that is subducted at the trench and that which is sequestered to the mantle. While temperature is assumed to have a first-order effect in our model, redox [*Libourel et al.*, 2003; *Li et al.*, 2016], pH [*Mikhail and Sverjensky*, 2014], and distribution between fluids and melt [*Li et al.*, 2015; *Mallik et al.*, 2018], may all have effects which are not considered here.

Thus, the flux of species subducted to the mantle is the product of subducted fraction, concentration in sediments or crust, and mass of sediments/crust subducted per year:

$$F_{\mathrm{subnet,j}} = f_{\mathrm{sub}} F_{\mathrm{subT,j}}. \tag{35}$$

for j ={all species}.

2.7.2 Continental

That which is not subducted will either be outgassed at arcs (F_{ogarc}) or be incorporated into the continental crust (F_{cg}). All Ar is outgassed, all K and PO_4^{3-} goes into the continental crust. For N, f_{Ncgarc} is set to 0.5. That is, half of N released from subducted materials is outgassed at arcs and half is incorporated into the continental crust. This value, 0.5, is an assumption in our model. There is very little data concerning N in subduction zones that is released from the slab. Nitrogen isotopes in granites indicate a biologic source [*Boyd*, 2001; *Johnson and Goldblatt*, 2017], which could be from subducted material. More analysis of granitic rocks would help characterize this flux. Thus:

$$F_{\mathrm{cg},j} = (1 - f_{\mathrm{sub}}) F_{\mathrm{subT,j}} \tag{36}$$

for j ={K,^{40}K,^{40}Ar,^{36}Ar} and

$$F_{\mathrm{cg,N}} = f_{\mathrm{Ncgarc}} (1 - f_{\mathrm{sub}}) F_{\mathrm{subT,N}} \tag{37}$$

for N. All subducted PO_4^{3-} is added to the continental crust.

Species in the continental crust have a residence time of 300 Myr, or time constant (τ_w) of 3.33×10^{-9} yr^{-1}, which is equivalent to half a Wilson cycle [*Nance and Murphy*, 2013]. Weathering efficiency depends on atmospheric O_2, with weathering increasing with increasing O_2:

$$W_{\mathrm{eff},j} = \tau_{\mathrm{w}} \left(a_{\mathrm{W}} + (1 - a_{\mathrm{W}}) \frac{PAL_{\mathrm{O2}}}{PAL_{\mathrm{O2}} + k_{\mathrm{weath}}} \right) \tag{38}$$

Where a_{W} is the fraction of available material weathered under anoxic conditions (0.1), PAL_{O2} is atmospheric O_2 compared to present atmospheric levels, and k_{weath} is a weathering rate constant (1×10^{-3}). Weathered^{36}Ar and^{40}Ar are released to the atmosphere, while all other species (N, PO_4^{3-}, K) are added to the shelf ocean. As there is no crustal organic

material in the model, all continental N is weathered as NH_4^+, which is the mineralogically most stable form of N. Weathering (F_w) is parameterized as:

$$F_{w,j} = W_{eff} R_j^{contcrust} \tag{39}$$

2.8 Mantle

Species are added to the mantle at subduction zones (F_{subnet}). It is assumed that they instantly homogenize into the mantle (i.e., there are no separate mantle domains). Species leave the mantle through degassing at mid-ocean ridges. Degassing is the product of the concentration (C_j^{man}) of the species in the mantle and the mass of mantle involved in crust genesis (M_{melt}). M_{melt} is set to 10 times the mass of oceanic crust produced (O_p), which and represents generation of crust by 10% partial melt (P_m). We assume 90% of all species are partitioned to the melt during partial melting (K_{dist}), with 10% remaining in the residual. We have chosen this partition of melt to residual to account for the observation that mantle rocks that have undergone some melting still have low, but measurable N of less than 1 ppm [*Johnson and Goldblatt*, 2015, and references therein]. Thus, mid-ocean ridge outgassing is:

$$F_{ogmor,j} = C_j^{man} P_m O_p K_{dist}. \tag{40}$$

We note that there is no explicit treatment of intra-plate, or hot spot, volcanism in the model. In addition, we do not distinguish between the upper mantle, transition zone, and lower mantle. There are redox changes with depth in the mantle [e.g. *Frost and McCammon*, 2008], which have important effects on N solubility in mantle minerals [*Li et al.*, 2013, 2016]. As discussed in *Li et al.* [2013] and *Johnson and Goldblatt* [2015], the mantle likely has an enormous capacity for N, which likely exceeds its actual content at any given time. Future modeling work including mantle structure and redox evolution would be an important addition to the work shown herein.

2.9 Details on code structure

The model code was constructed to prioritize flexibility. Due to the high number of unknowns in the system, giving flexibility was important. We set up the reservoir book-

keeping as a structure array in Matlab. This allows for dynamic field names to be used, which assists in ease of code reading. We also constructed it so that initial conditions are read in through a separate text file. This allows easy changes, but it is also flexible as not every species has to be in every box. It also calculates ^{40}K from K initial conditions, reducing input time and error.

The differential equation file is arranged so that it is straightforward to turn various fluxes off and on. The purpose for this design is that this model, or one like it, could be used for not only Earth history, but could be applied to planetary evolution in general. Different planetary evolution pathways may or may not involve subduction, different atmospheric compositions, or differing biologic pathways and metabolisms. Testing the response of the system to such differences, perturbations, and the presence or absence of one or more fluxes could be of great value in studying planetary evolution.

In detail, we used Matlab's ode15s solver. This is a variable-step, variable-order solver that uses numerical differentiation formulas of orders 1 to 5. We set the relative error tolerance to 1×10^{-7} and a maximum step size of 10^6 years. Code is available in the supplementary material. Please contact us if you wish to use this code in order to obtain the latest version.

3 Results and Discussion

We ran the model in all runs for 4.5 Ga, after a spin up period of 10 Myr to equilibrate atmosphere, ocean, and sediment boxes. All biologic N fluxes are "available" at each model step.

3.1 Nominal Run

In order to test the effects of different conditions over Earth history, such as oxygenic photosynthesis evolution time and style of mantle cooling, we first describe the results of a nominal model run.

This realization is based on a conservative set of assumptions regarding initial and boundary conditions and choice of parameterizations (Fig. 3). Mantle cooling and mid-ocean ridge crust production (i.e., mid-ocean ridge outgassing) is from *Korenaga* [2010], with the fraction of subducted N retained to the deep mantle dependent on mantle temperature. The atmospheric O_2 history is prescribed, and oxygenic photosynthesis evolves at

418 2.8 Ga. Plate tectonics starts at 3.5 Ga, continental weathering timescale is 300 Myr, and
419 hydrothermal alteration is parameterized as a fixed volume flow (1.6 Sv).

420 We estimate the proportions of N that start in the atmosphere and the mantle at the
421 end of the magma ocean phase of Earth history, and use this as the initial condition for
422 the nominal run (Appendix B:). Using results from *Libourel et al.* [2003], which relates
423 pN_2 to N dissolved in basaltic magma, and a mantle fO_2 of IW-2 [*Wood et al.*, 2006],
424 which is expected at the end of core formation, we calculate N_2 concentration in a magma
425 ocean for a range of atmospheric pN_2 values. We assume the entire mantle experienced
426 a magma ocean phase. Then, given this relationship, we can estimate a total N budget
427 and what proportion of that N starts in the atmosphere and the mantle. We select a total
428 N budget for the nominal run to be consistent with budget estimates from *Johnson and*
429 *Goldblatt* [2015], and one that reproduces the current distribution of N in the atmosphere
430 (1 PAN) and the mantle (>3 PAN). Our starting conditions are therefore total N of 4.8
431 PAN, with 80% starting in the atmosphere and 20% in the mantle. The evolution of major
432 N reservoirs (atmosphere, mantle, continental crust, ocean sediments) is shown in Fig. 4
433 with atmosphere-ocean gases and nutrients shown in Fig. 5.

Table 4: Nitrogen reservoir and flux comparisons: nominal model output results compared to literature N mass estimates from *Johnson and Goldblatt* [2015], with continental crust from *Johnson and Goldblatt* [2017]. Reservoirs are in units of 10^{18} kg N, while ocean concentrations are shown in μM. Shallow ocean model results are the average of low-latitude, high-latitude, and shelf boxes. Deep ocean values from the literature are for 1000 m depths. Model values are from the end of nominal model run (i.e., modern values). Fluxes are in Tmol N yr^{-1} unless otherwise noted. Model results are shown for modern day reservoir fluxes.

Reservoir/Flux	**Model**	**Literature**	**Reference**
Atmosphere	3.92	4	*Johnson and Goldblatt* [2015]
Mantle	12	24 ± 16	*Johnson and Goldblatt* [2015]
Continental Crust	1.8	1.7 – 2.7	*Johnson and Goldblatt* [2015, 2017]
Oceanic Lithosphere	0.05	0.2 ± 0.02	*Johnson and Goldblatt* [2015]
Total ocean Sediments	1.2	0.41 ± 0.2	*Johnson and Goldblatt* [2015]
Shallow ocean NO_3^-	22	7	*Gruber* [2008]

Continued on next page

Table 4 Reservoir comparison – continued from previous page

Reservoir/Flux	Model	Literature	Reference
Deep ocean NO_3^-	25	31	*Gruber* [2008]
Shallow ocean NH_4^+	2.4	0.3	*Gruber* [2008]
Deep ocean NH_4^+	1.5	0.01	*Gruber* [2008]
Shallow ocean PO_4^{3-}	0.12	< 1	*Garcia et al.* [2014]
Deep ocean PO_4^{3-}	0.36	$1 - 3$	*Garcia et al.* [2014]
Shallow ocean O_2	533	$220 - 400$	*Garcia et al.* [2014]
Deep ocean O_2	530	$40 - 400$	*Garcia et al.* [2014]
Biologic fluxes			
N-fixing	6.4	13	*Gruber and Galloway* [2008]; *Vitousek et al.* [2013]
Nitrification	19	85	*Gruber* [2008]
Denitrification	6	22	*Gruber* [2008]
N-remineralization	21	93	*Gruber* [2008]
Geologic Fluxes			
Continental weathering	0.43	1.1	*Houlton et al.* [2018]
Burial/sedimentation	0.73	0.07	*Gruber* [2008]
Total subduction	0.66	0.0064	*Mallik et al.* [2018]
		0.0094	*Busigny et al.* [2011]
		0.1	*Halama et al.* [2014]
Arc outgassing	0.08	0.0375	*Catling and Kasting* [2017]
Mid-ocean ridge outgassing	0.2	0.0038	*Catling and Kasting* [2017]
Total outgassing	0.28	0.09	*Catling and Kasting* [2017]

We focus first on model output at the modern day. The nominal run reproduces the modern atmospheric and estimated mantle N masses well. The mantle value, specifically, is somewhat lower, but within the estimated mantle N budget from *Johnson and Goldblatt* [2015], which is 7 ± 4 PAN. The nominal run has 3.25 PAN in the mantle at modern. We present full comparisons with values from the literature in Table 4.

Model output is consistent with estimates for the modern day N budget in deep sediments of ~ 0.1 PAN [*Johnson and Goldblatt*, 2015], and continental crust. For example, recent work using glacial tills as a proxy for upper continental crust through time suggest a secular increase in crustal N during the Precambrian [*Johnson and Goldblatt*, 2017]. The authors suggest that isotopic evidence is most consistent with this addition of N to the continents being biological in origin. Atmospheric N is biologically fixed and then subsequently added to the continents either via collision of marginal marine sediments or incorporation from subduction zone processing, with a total crust N content of 0.5-0.67 PAN. While we do have both of these fluxes in our model, they are only very general. It is well known that the Earth has gone through periods of orogenic activity and periods of quiescence [e.g., *Condie*, 2013] with variable passive margin extent [*Bradley*, 2008], and these variations are not captured in our model.

In all model runs, prior to the evolution of oxygenic photosynthesis the N cycle is marked by mantle degassing and atmospheric N growth, after a period of atmospheric equilibration with oceanic sediments. (Figs. 4 - 6). High mantle temperatures, combined with low efficiency export production and N-fixing results in net mantle outgassing and atmospheric growth for the first 1.5 Ga of model output. Biologic N fluxes (Fig. 7) are low prior to oxygenic photosynthesis, due to lower overall productivity and burial. Then, coincident with, and caused by, the appearance of oxygenic photosynthesis, the atmosphere is drawn down, with an increase in all the geologic N reservoirs. Deep ocean sediments increase most quickly, with continental crust and the mantle increasing more slowly. At the GOE, an increase in weathering drives a spike in productivity and further atmospheric draw-down due to enhanced N-fixing. The Lomagundi-Jatuli type event, with high productivity, lasts for ~ 50 Myr. At about 1.6 Ga, the mantle and atmosphere have equal N budgets, and the mantle continues to increase at the expense of all other reservoirs until the present day.

While the nominal run reproduces modern N distribution well, there are discrepancies between modeled biologic and geologic fluxes and estimates of these fluxes from the literature (Fig. 4). The model somewhat underestimates N-fixing, nitrification, and denitrification. It is possible to explain some of this discrepancy by the lack of continental biologic N-cycling in our model, since at present continental ecosystems account for half of global biologic N cycling [e.g., *Gruber and Galloway*, 2008]. Similarly, nominal output for

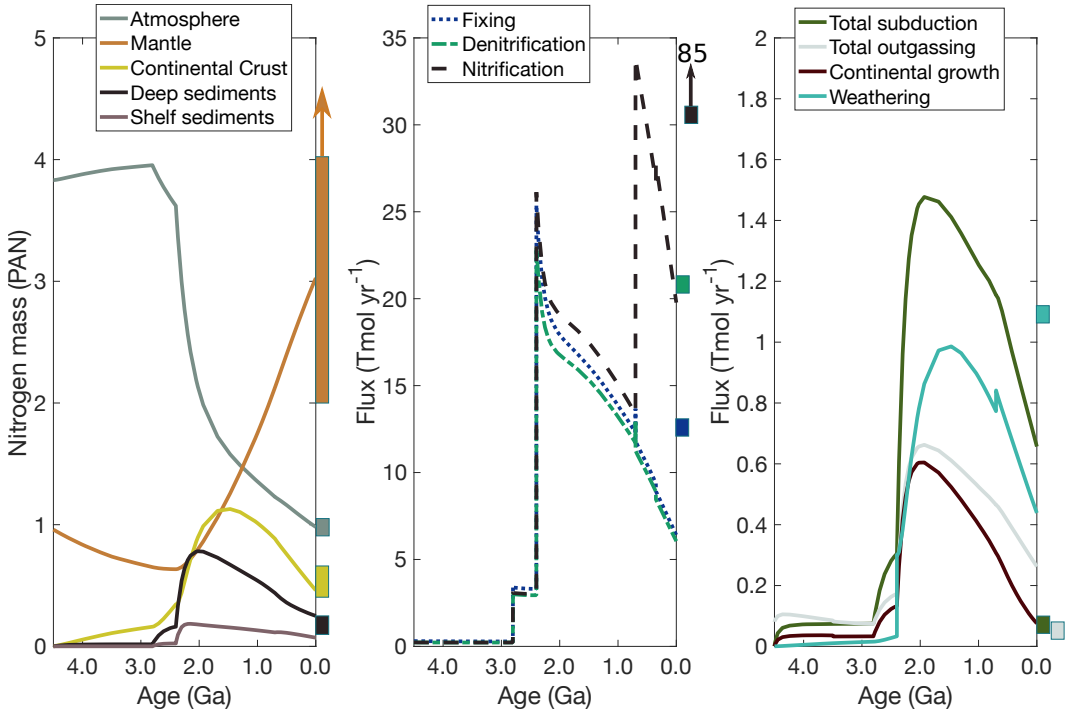

Figure 4: a. Nitrogen reservoirs through time from a nominal run. b. Biologic nitrogen fluxes and c. Geologic fluxes. Estimates for modern amounts are shown as colored bars next to each panel [*Gruber*, 2008; *Gruber and Galloway*, 2008; *Busigny et al.*, 2011; *Vitousek et al.*, 2013; *Halama et al.*, 2014; *Johnson and Goldblatt*, 2015; *Catling and Kasting*, 2017; *Mallik et al.*, 2018; *Houlton et al.*, 2018].

continental N weathering is less than a recent study [*Houlton et al.*, 2018]. Adding more explicit treatment of continental N cycling would be a welcome addition to this model.

For the other major geologic fluxes, outgassing and subduction, the EarthN model output is higher than estimates from the literature. This indicates that either subduction of N is not as efficient as we describe, and recycling into the mantle is less, or literature estimates of subduction and outgassing are too low. It is notoriously difficult to estimate N fluxes outgassing at subduction zones and mid-ocean ridges [*Fischer et al.*, 2002; *Elkins et al.*, 2006], due to high background atmospheric N_2. In addition, there are very few estimates of N cycling in subduction zones [*Fischer et al.*, 2002; *Elkins et al.*, 2006; *Mitchell et al.*, 2010; *Halama et al.*, 2014; *Mallik et al.*, 2018], and it is possible that this flux is being underestimated in the literature due to the difficulty in analyzing silicate-bound N.

3.1.1 Ocean nutrients through time

Our results yield several important predictions of nutrient content of the ocean through time. First, and unsurprisingly, $NH_4^+$is the dominant bioavailable N species in the ocean, and PO_4^{3-} remains high ($\sim 1-3\ \mu$M) before oxygenic photosynthesis. Second, after the appearance of oxygenic photosynthesis and the associated increase in productivity (Fig. 3), burial increases. The increase in burial is reflected in the increase in N in ocean sediments and in all biologic N fluxes (Fig. 4). We note here that since we do not include abiotic N-fixing, and instead assume biologic N-fixing could operate throughout the model run, we might be slightly overestimating early Archean N-fixing if biologic fixing did not evolve till 3.2 Ga [*Stüeken et al.*, 2015]. For example, *Navarro-González et al.* [2001] suggests 2.1×10^{10} mol yr^{-1} could be fixed abiotically by lightning, while the minimum N-fixing we calculate is 2.9×10^{11} mol yr^{-1}. At the same time as the increase in N-cycle fluxes, PO_4^{3-} concentrations drop an order of magnitude, again the result of increased productivity and burial. We also note that there is a small oxygen oasis in the shelf ocean box, which is consistent with evidence for localized oxic conditions prior to widespread oxygenation at the GOE [*Anbar et al.*, 2007] Additionally, nutrient concentrations increase after the GOE, as the result of increased weathering efficiency.

Third, NH_4^+ and NO_3^- are at about the same concentration in the Proterozoic. This balance is the result of O_2 levels, and so is dependent on our O_2 forcing scheme, which sets Proterozoic O_2 levels at 1% of modern. There is not agreement on the exact level of O_2 in the Proterozoic [*Lyons et al.*, 2014; *Planavsky et al.*, 2014; *Reinhard et al.*, 2016; *Zhang et al.*, 2016], but generally the maximum estimates are no greater than 10% of modern. Thus, the transition to a NO_3^--rich ocean is predicted to only occur at the NOE, and our modeling does not indicate any sort of N-limitation during the Proterozoic. We do not, however, model a specific increase in productivity due to the evolution of eukaryotes, which might be expected to enhance biologic N-cycling [e.g., *Zerkle and Mikhail*, 2017, and references therein].

3.1.2 Different plate tectonic histories

Different mantle cooling history could have a large effect on the transfer and sequestration of N from the surface into the mantle over time. For example, if mantle temperatures were hotter in the Archean, one might expect both faster mantle convection and less

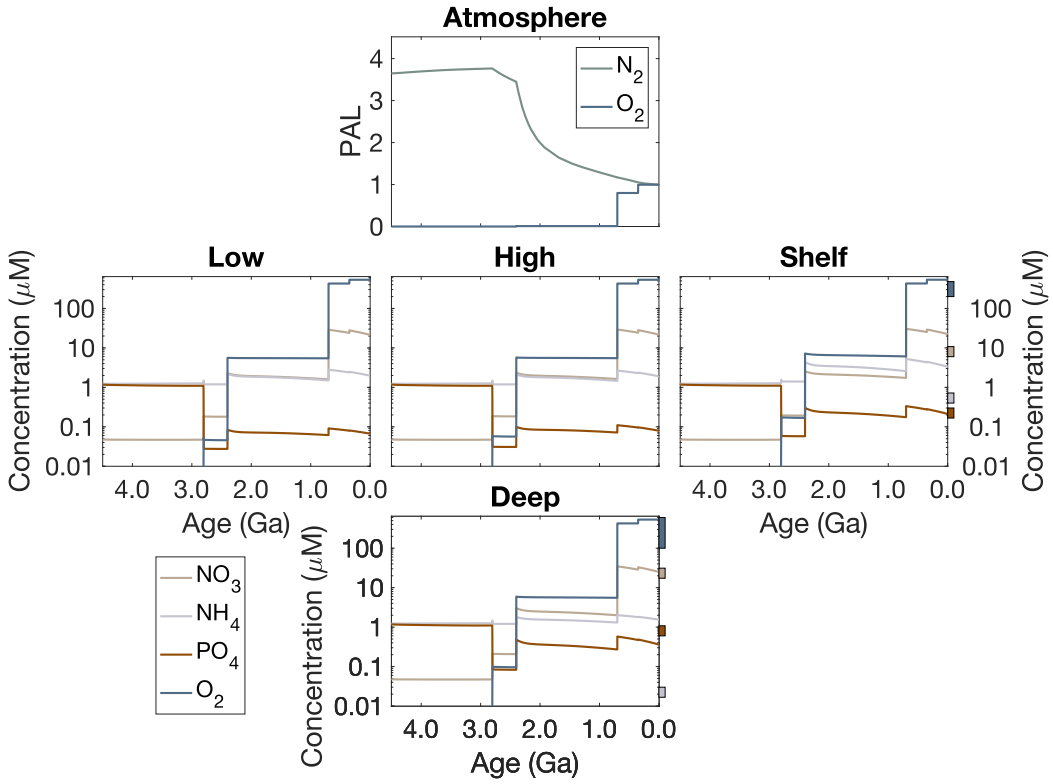

Figure 5: Nitrogen, O_2, and PO_4^{3-} surface reservoirs through time for a nominal run. $NH_4^+$is the dominant N species until the Neoproterozoic Oxygen Event, and PO_4^{3-} is high until the evolution of oxygenic photosynthesis. A small O_2 oasis exists in the late Archean shelf ocean. Literature estimates for modern values are shown as colored bars next to shallow boxes; the shallow ocean bars are for the average shallow ocean, and deep ocean represents 1000 m depth [*Gruber*, 2008; *Garcia et al.*, 2014].

efficient retention of N at subduction zones. Relatedly, if mantle temperature is not the main control on N retention into the mantle at subduction zones, different subduction efficiencies would lead to correspondingly different N histories.

To test these possibilities, we ran the model with three different styles of mantle cooling/plate tectonic transfer of N from the surface to the mantle (Fig. 6). The first, as described in the nominal run section, is based on *Korenaga* [2010]. In the second, mantle temperature, ocean crust production, and subducted crust are all constant, set to the average of each value from *Sandu et al.* [2011], which uses a "canonical" mantle cooling. In

addition, the fraction of subducted N that is transported to the deep mantle is held constant at 0.2. In the third realization, we allow subducted fraction to vary with canonical mantle evolution temperature.

In all three realizations, prior to oxygenic photosynthesis, there is net mantle outgassing and atmospheric growth. Similarly, after oxygenic photosynthesis and more efficient export production, there is net atmospheric drawdown into geologic reservoirs. The amount of drawdown by subduction with canonical mantle cooling, with either constant or temperature-linked efficiency, is more overall than in the nominal run, up to 4 PAN in the latter. Constant subduction efficiency, however, cannot sequester enough atmospheric N into the mantle to result in a 1 PAN atmosphere at modern. In addition, this run results in more N in the atmosphere than the mantle, contradicting estimates of N distribution on Earth today [*Johnson and Goldblatt*, 2015]. Interestingly, the overall pattern is insensitive to mantle cooling history.

We also explored realizations where the time of plate tectonic initiation and oxygenic photosynthesis were varied (Fig. 7). The initiation of plate tectonics does not affect the overall pattern, nor does it greatly effect the distribution of N between various reservoirs. Mantle cooling, and its effect on subduction efficiency, has a larger effect than timing of plate initiation alone. Similarly, only when biologic productivity increases after oxygenic photosynthesis do major changes in N distribution occur.

3.1.3 Different oxygenic photosynthesis appearance

Another main "knob" on the control panel of the N cycle is how biologic activity processes this in the oceans. As seen in the nominal run, the appearance of oxygenic photosynthesis and the GOE exert a large control over how active N-fixing, nitrification, and denitrification are. To test for any effects of different times of oxygenic photosynthesis evolution (Fig. (Fig. 7), we ran the model with standard conditions, but altered when oxygenic photosynthesis evolves: early (3.5 Ga), middle (2.8 Ga, standard), and late (2.4 Ga). These times were chosen to coincide with early fossil evidence for photosynthetic life [*Hofmann et al.*, 1999], molecular and geochemical evidence for oxygenic photosynthesis by 2.8 Ga [see *Buick*, 2008], and the GOE at 2.4 Ga [*Farquhar et al.*, 2000].

In all runs, when oxygenic photosynthesis evolves, atmospheric N is drawn down. Initially, N is sequestered into deep sediments, then, if plate tectonics is operating, sent

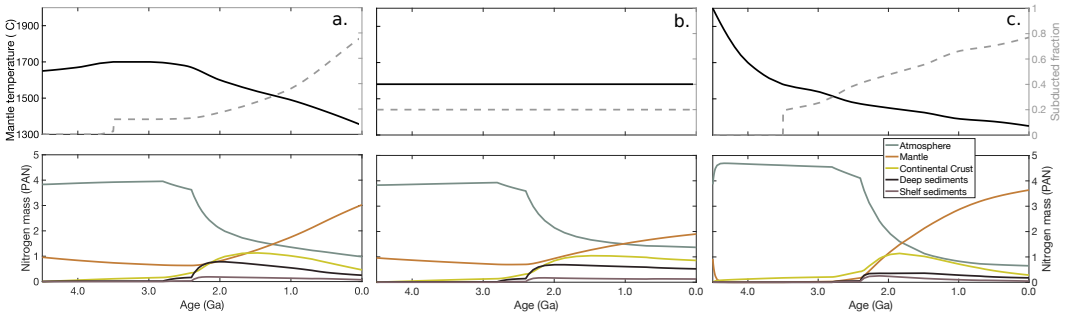

Figure 6: Nitrogen reservoirs and subducted fraction for different subduction parameters. a.) nominal run, b.) constant subduction, c.) canonical subduction. The Archean in all cases is characterized by net mantle outgassing, but outgassing is rapid in canonical subduction runs. Net drawdown occurs after oxygenic photosynthesis evolves, and deep sediments and continental crust increases as well.

into the mantle and continental crust. If oxygenic photosynthesis appears later, atmospheric N reservoir reaches a slightly higher maximum prior to drawdown. In addition, all else being equal, a later appearance of oxygenic photosynthesis results in a slightly higher pN_2 at modern. Overall, the main change in N-history occurs at the GOE, driven by increased weathering, nutrient supply, and enhanced biologic productivity.

3.2 Atmospheric pN_2 comparison with other reconstructions

As mentioned in the introduction, there is a discord between modern geochecmical data suggesting net ingassing of the atmosphere through time [*Busigny et al.*, 2011; *Nishizawa et al.*, 2007; *Barry and Hilton*, 2016] and either net outgassing [*Som et al.*, 2012, 2016] or atmospheric stability since the Archean [*Marty et al.*, 2013]. Our model strongly suggests dynamic behavior over time, with the N distribution on Earth responding to changes in biologic and geologic evolution over time.

In order to match constraints for similar or lower atmospheric N mass in the past [*Marty et al.*, 2013; *Som et al.*, 2012, 2016], but still end up with a 1 PAN modern atmosphere, our model has to be tuned to very specific parameters (Fig. 8) within an otherwise nominal run. Given our standard total N budget (4.8 PAN), the mantle must start with the majority (90%) of total N, due to net outgassing during the Hadean and Archean. In addition, the net subduction of N at subduction zones has to be low and constant (10%), as an

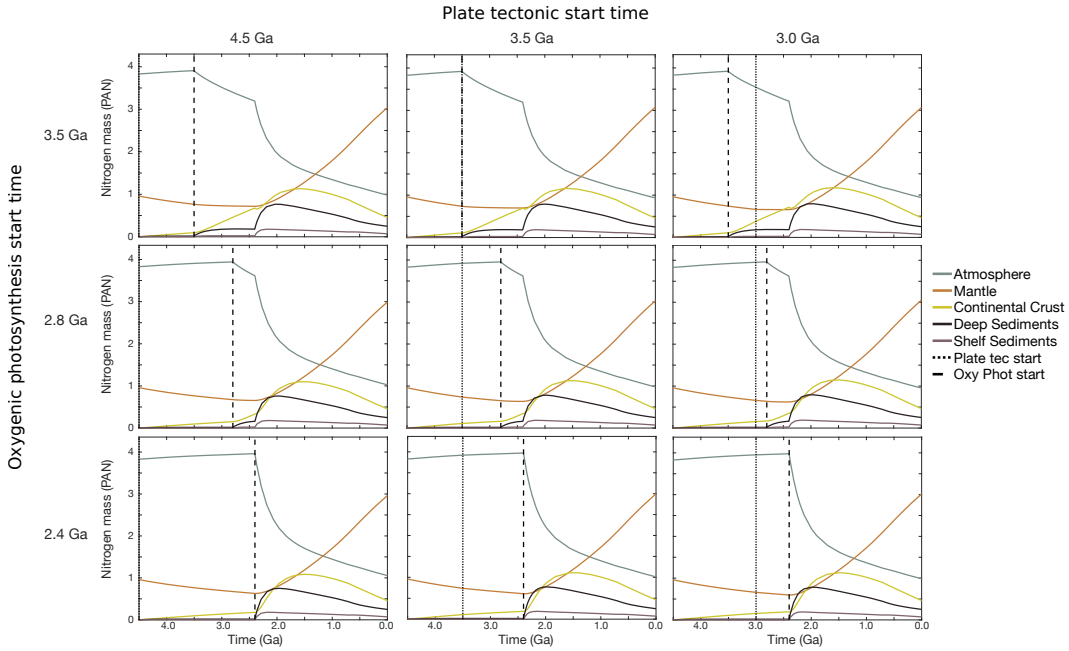

Figure 7: Nominal runs varying plate tectonic (4.5, 3.5, 3.0 Ga) and oxygenic photosynthesis starting time (3.5, 2.8, 2.4 Ga). The overall pattern for major N reservoirs is similar for all cases. Mantle N increases when subduction begins, atmospheric drawdown of N into ocean sediments occurs when oxygenic photosynthesis evolves, and further drawdown occurs after the GOE.

increase in net subduction over time results in atmospheric drawdown in all model runs. We also have to increase hydrothermal circulation from 5 to 50 Sv, which limits PO_4^{3-} and in turn limits atmospheric drawdown via N-fixing. The model with these parameters can reproduce the constraints of 1 PAN at 3.46 Ga [*Marty et al.*, 2013] and a 0.5 PAN atmosphere at 2.7 Ga [*Som et al.*, 2012, 2016] but still result in a 1 PAN modern atmosphere. Even in this case, there is still a 1.75 PAN atmosphere at 2.8 Ga, when oxygenic photosynthesis evolves. The atmosphere undergoes a dynamic evolution.

Lower atmospheric mass in the past cannot be specifically ruled out by our model output, but such lower mass would present a number of interesting implications. The lack of evidence for large glaciations in the Archean is difficult to reconcile with low atmospheric mass [*Goldblatt et al.*, 2009]. Similarly, the majority of the Proterozoic, or "boring billion", lacks evidence for glaciation, implying warm climate. If the Earth had less than a one PAN atmosphere, there would need to be $10^{-2.2}$ bars of CO_2, and even more with less N.

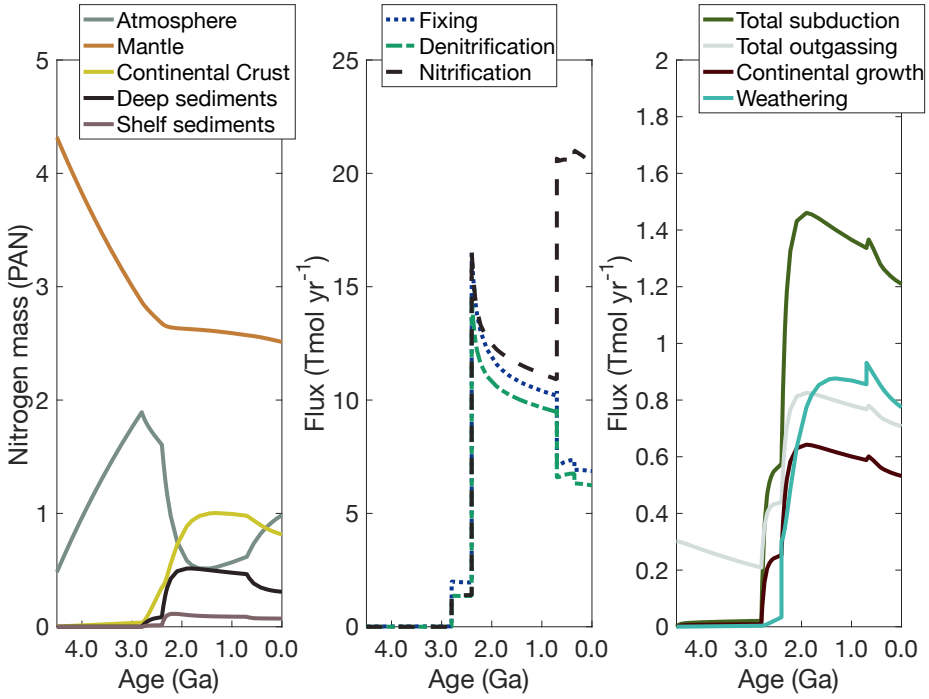

Figure 8: Nominal run but with low starting atmospheric mass, 5% starting N in the atmosphere, constant net subduction (10%), and high (50 Sv) hydrothermal circulation. These conditions lead to a model realization consistent with previous estimates of a 1 PAN atmosphere at 3.46 Ga [*Marty et al.*, 2013] and 0.5 PAN at 2.7 Ga [*Som et al.*, 2012, 2016].

3.3 Investigating unknown nitrogen distribution: Monte Carlo simulations

Despite recent interest in geologic and Earth system N cycling [*Johnson and Goldblatt*, 2015; *Zerkle and Mikhail*, 2017; *Johnson and Goldblatt*, 2017], there is not a consensus on how much N the Earth contains and how it has moved between different reservoirs over time. In addition, and especially in the Hadean and Archean, a number of parameters that could affect the N cycle are not well constrained. These include when oxygenic photosynthesis first appeared, the rate of hydrothermal alteration of ocean crust, deep water upwelling, continental weathering, and the initiation of plate tectonics [*Van Hunen and Moyen*, 2012]. To investigate how changing these poorly constrained parameters may have affected the N cycle over time, we ran Monte Carlo simulations (n=1000) where a number of parameters were given random values within a prescribed range (Table 5, Figs. 9-10).

Table 5: Range of values used for Monte Carlo simulartions. PAN is Present Atmospheric Nitrogen, or 4×10^{18} kg

Parameter	**Range (units)**
Upwelling	0.16–16 Sv
Oxygenic photosynthesis start time	2.4-3 Ga
Plate tectonics start time	3-4 Ga
Weathering timescale	50-500 Myr
Hydrothermal flow rate	0.5-50$\times 10^{16}$ L yr^{-1}
Total N	2-12 PAN
Percent starting in atmosphere	0-100%

Strikingly, our model suggests that the amount of N found in the atmosphere today may in some part be related to the total N in the planet (Fig. 9). There is a strong correlation between the total N in the model and the atmospheric N mass after 4.5 Gyr of planetary evolution. Monte Carlo results that have 1 PAN atmosphere at the present day are those with a total N budget of $\sim 4 - 6$ PAN, similar to independent budget estimates [*Johnson and Goldblatt*, 2015]. On Earth, the atmospheric N content directly relates to the total planetary N budget. It is possible that this proxy may work for other terrestrial plan-

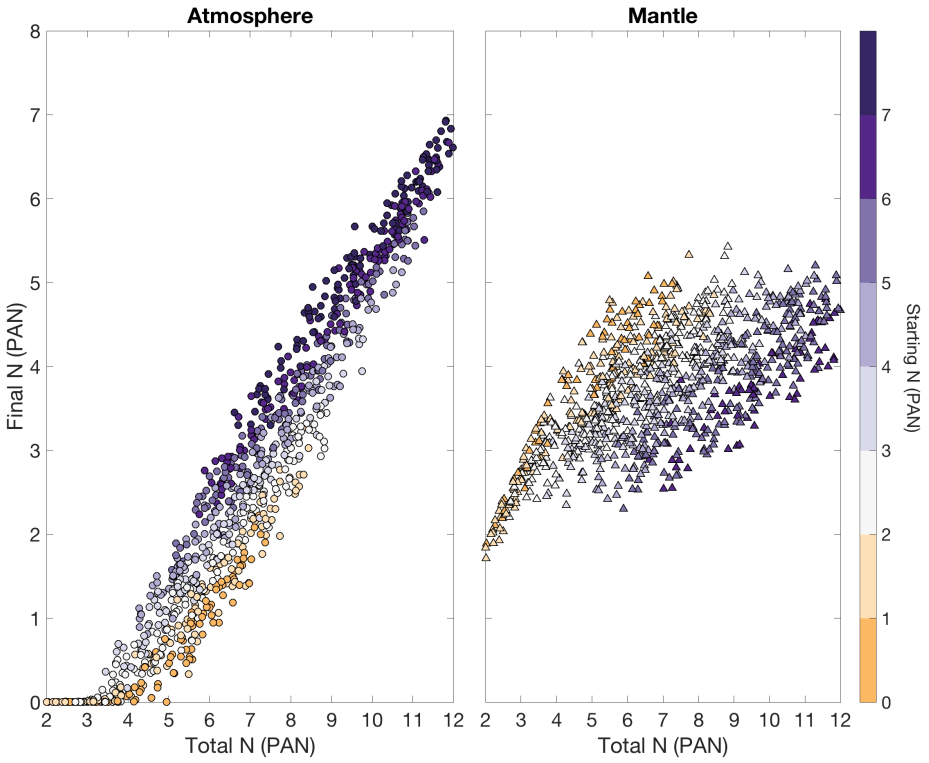

Figure 9: Final atmospheric and mantle N vs total N for 1000 Monte Carlo simulations. Note strong correlation between atmospheric N and total N, and that for very low N budgets, the atmospheric mass is small. Runs that results in a 1 PAN atmosphere have 5 PAN total N. The mantle saturates at 3 PAN.

ets, given evidence for plate tectonics (e.g., linear mountain belts, bimodal topographies) and biologic N cycling (e.g., N_2 and O_2 coexisting, N_2O), atmospheric N could serve as an estimate for total planetary N content.

The mantle N content also increases with increasing total content, but tends to "saturate" at 4.5 PAN (Fig. 10). This is because net subduction and outgassing at mid-ocean ridges tend to balance each other, while N-fixing is limited by PO_4^{3-} availability. That is, the rate at which organisms can fix N is not enough to outpace overall outgassing, thus at higher total N budgets, N accumulates in the atmosphere. For very small total N budgets less than 3 PAN, N-fixing is efficient enough to draw down the atmosphere almost completely into the mantle.

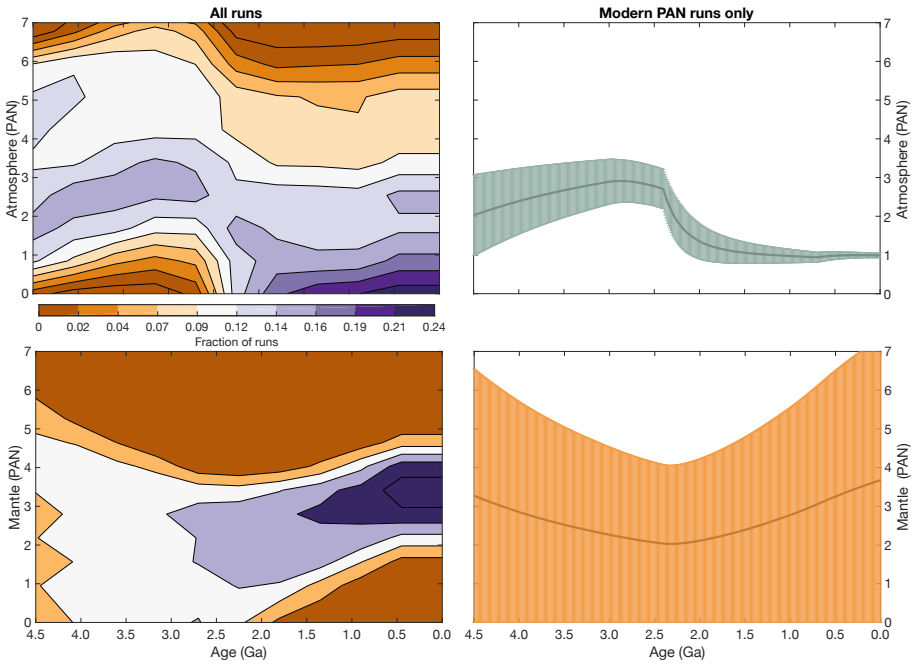

Figure 10: Results of Monte Carlo runs for atmosphere and mantle values through time for all runs (a-b) and just runs that result in a 1 PAN present atmosphere (c-d). Panels c-d show the mean and one standard deviation. The mantle tends to evolve towards a final value of between 3-4 over time, while the atmosphere is more variable. Most runs end with a 2 PAN atmosphere at modern and throughout much of the Proterozoic and Archean, with two other nodes at 0.5 and 4 PAN. Runs that result in a 1 PAN atmosphere start with a $\sim$ 2 PAN atmosphere at 4.5 Ga,, and are drawn down in the late Archean. Mantle N for runs that result in a 1 PAN atmosphere average 4 PAN, but are variable.

In addition, the EarthN model does not thoroughly parameterize mantle evolution over time. Thus, we predict that model output suggesting mantle saturation at 4.5 is a minimum estimate of the true N content of the mantle.. Previous work has estimated that the mantle has an enormous capacity for N, and could possibly contain many 10s of PAN [*Li et al.*, 2013; *Smith et al.*, 2014; *Johnson and Goldblatt*, 2015].

Monte Carlo realizations that result in a 1 PAN present atmosphere show the same overall pattern as the nominal run (Fig. 10). On average, the atmosphere starts out with greater than modern mass, then decreases, again likely due to the evolution of oxygenic photosynthesis, in the late Archean. The atmosphere remains at approximately 1 PAN

throughout the Proterozoic, with a small increase at the NOE, due to enhanced denitrification at this time. Even when we allow for a random total N and a random amount of N starting in the atmosphere, the overall trend in the atmospheric evolution is to be drawn down from higher Archean values towards the modern. In contrast, the mantle stays consistent on average, at its saturation of about 4 PAN. The standard deviation shown in Fig. 10-d indicates there are many mantle N paths which are consistent with the EarthN model evolving a 1 PAN present atmosphere.

As previously mentioned, the temperature history of the mantle, and behavior of N in different geothermal regimes exerts a strong control on the evolution of N in the Earth system over time. This behavior also depends on how much temperature actually controls N volatilization at subduction zones. Studies have shown that redox [*Li et al.*, 2013], temperature/pressure [*Li and Keppler*, 2014], distribution of N between fluid and melt [*Mallik et al.*, 2018], and pH [*Mikhail and Sverjensky*, 2014] also exert control over N speciation and retention in the mantle. The interaction of these different factors in geologic evolution could have had a large effect on N cycling over Earth history [*Mikhail and Howell*, 2016]. We predict that redox evolution is likely to have the largest effect on N processing and storage in the mantle. The upper mantle and mantle lithosphere have, on average, been at their current redox state since 3.5 Ga [*Canil*, 2002]. Arc basalts, however, are more oxidized than MORBs with otherwise similar chemical composition [*Kelley and Cottrell*, 2012; *Brounce et al.*, 2014]. In addition, the deeper mantle is more reducing than the upper mantle [*Frost and McCammon*, 2008].

It follows, then, that N is more soluble in the reduced lower mantle than the more oxidized upper mantle and subduction zone mantle wedge. As the mantle has become more oxidized through time, N recycling to the atmosphere would be favored. If the oxidation state of subduction zone mantle has similarly increased through time, this would enhance recycling of N to the surface [e.g., *Mikhail and Sverjensky*, 2014]. Thus, there are competing features controlling N recycling into the mantle: decreasing temperature and increasing fO_2. Given observations of net N retention at modern subduction zones [*Li et al.*, 2007; *Mitchell et al.*, 2010; *Halama et al.*, 2014], we hypothesize that mantle wedge temperature is the dominant control of N recycling efficiency, at least on the modern Earth. How this balance of redox and temperature has controlled N, and other volatile, recycling over Earth history has important implications for the evolution of the surface and interior of the planet.

The above discussion highlights a broader point regarding model construction. Herein, we have constructed an Earth system N cycle model, and presented a nominal run based on plausible assumptions about the Earth through time. The results presented, however, should not be taken as gospel, dogma, or actuality. There are a number of fluxes and factors in the Earth which could affect results of the EarthN model. In addition to mantle chemistry, mantle capacity for N is enormous [*Li et al.*, 2013], and the great potential size of this reservoir could have major influence over N cycling during Earth history. The lack of continental ecosystems, and simple treatment of hydrothermal activity in oceanic crust in this model could be important parameters to investigate. The addition of isotopes to the model would allow for predictions that could be tested in the rock record. We envision future studies to explore this wider parameter space, both for specific intervals in time and for grand trends over Earth history.

4 Conclusions

We have constructed an Earth system N model, EarthN, that includes biologic and geologic fluxes to predict the distribution of N in the major reservoirs of the Earth through time. In addition to linking the N cycle to PO_4^{3-} availability, the model is driven by changing O_2 abundance and mantle cooling with plate tectonics. Model output is consistent with movement of N between the three major reservoirs (atmosphere, mantle, continental crust) in significant amounts over Earth history.

In all model runs, the early part of Earth history, from 4.5-2.8 Ga, is characterized by net mantle outgassing and atmospheric growth. This early history is due to high mantle temperatures and inefficient export production. After the evolution of oxygenic photosynthesis, atmospheric N is immediately drawn down and sequestered in sediments due to increased export production. At the Great Oxidation Event, increased weathering and nutrient delivery enhances export production, which in turn enhances atmospheric drawdown via N-fixation. Mantle cooling over time, with associated increase in efficiency of N subduction, facilitates biologically fixed N to be sequestered into geologic reservoirs over time.

One of the strongest controls on the atmospheric mass of N through time, and especially the modern mass of the atmosphere, is the total N in the Bulk Silicate Earth. Monte Carlo simulations that vary a number of parameters (deep water upwelling, hydrothermal

687 circulation, oxygenic photosynthesis appearance, weathering timescale, total N and distri-
688 bution) that result in a 1 PAN atmosphere after 4.5 Ga of model evolution are most con-
689 sistent with a total BSE N budget of $\sim 4 - 6$ PAN. The mantle tends to saturate at 4-4.75
690 PAN. The mantle is the dominant N carrier for total N budgets below 6-7 PAN, while the
691 atmosphere is dominant at higher values.

692 The EarthN model shows that the distribution of N in the Earth system through time
693 could have varied significantly. Nominal model runs result in net atmospheric drawdown
694 over time, which is consistent with geochemical proxies. There are a number of controls
695 on N history, including appearance of oxygenic photosynthesis, mantle cooling, and N in
696 subduction zones. We anticipate further work in this area to focus on how temperature
697 and redox control N at subduction zones. Equally, the cycling of N in the mantle over
698 time is poorly known but crucially important. There is potential for not only investigating
699 Earth history, but exploration of Venus, Mars, and potential exoplanetary targets in the
700 future.

701 **Acknowledgments**

702 The authors would like to acknowledge Katja Fennel for sharing code. We also acknowl-
703 edge helpful discussions concerning model development with Rameses D'Souza, Arlan
704 Dirkson, and Christiaan Laureijs at the University of Victoria. Ananya Mallik and one
705 anonymous reviewer are thanked for useful reviews, as is Cyn-Ty Lee for editorial duties.

706 Supporting model code and output data can be found as a supplemental file with
707 this manuscript. In addition, code will be available at the corresponding author's webpage:
708 www.benwjohnson.com.

709 BWJ is currently supported by NSF (EAR - 1725784) and was previously supported
710 by NSERC Discovery grant to CZG. CZG is supported by an NSERC Discovery grant.
711

712 **A: Differential equations**

713 Based on the above model decsription, we write a series of differential equations to
714 solve for model species in boxes.

Atmosphere

$$\frac{dR_j^{\mathrm{atm}}}{dt} = \sum_{i*} F_{\mathrm{as,j}}^{atm-i*} + F_{\mathrm{ogarc,j}} \tag{A.1}$$

for j ={N_2,^{40}Ar,^{36}Ar} and $i*$ includes air-sea flux from all shallow ocean boxes ({low, high, shelf}).

Low- and high-latitude shallow ocean

$$\frac{dR_{\mathrm{40Ar}}^i}{dt} = F_{\mathrm{mix,40Ar}}^i + F_{\mathrm{rd}}^i - F_{\mathrm{as,40Ar}}^{\mathrm{atm}-i} \tag{A.2}$$
$$\frac{dR_{\mathrm{36Ar}}^i}{dt} = F_{\mathrm{mix,36Ar}}^i - F_{\mathrm{as,36Ar}}^{\mathrm{atm}-i} \tag{A.3}$$
$$\frac{dR_{\mathrm{40K}}^i}{dt} = F_{\mathrm{mix,40K}}^i - F_{\mathrm{rd}}^i \tag{A.4}$$
$$\frac{dR_{\mathrm{K}}^i}{dt} = F_{\mathrm{mix,K}}^i \tag{A.5}$$
$$\frac{dR_{\mathrm{PO4}}^i}{dt} = F_{\mathrm{mix,PO4}}^i - F_{\mathrm{ExT}}^i \tag{A.6}$$
$$\frac{dR_{\mathrm{NO3}}^i}{dt} = F_{\mathrm{mix,NO3}}^i - F_{\mathrm{out,NO3}}^i + F_{\mathrm{nit}}^i - F_{\mathrm{den}}^i \tag{A.7}$$
$$\frac{dR_{\mathrm{NH4}}^i}{dt} = F_{\mathrm{mix,NH4}}^i - F_{\mathrm{out,NH4}}^i - F_{\mathrm{nit}}^i \tag{A.8}$$
$$\frac{dR_{\mathrm{N2}}^i}{dt} = F_{\mathrm{mix,N2}}^i - F_{\mathrm{out,N2}}^i + F_{\mathrm{den}}^i \tag{A.9}$$

for i ={low, high}.

Shelf ocean

$$\frac{dR_{\mathrm{36Ar}}^{\mathrm{shelf}}}{dt} = F_{\mathrm{mix,36Ar}}^{\mathrm{shelf}} - F_{\mathrm{as,36Ar}}^{\mathrm{atm\text{-}shelf}} \tag{A.10}$$
$$\frac{dR_{\mathrm{40Ar}}^{\mathrm{shelf}}}{dt} = F_{\mathrm{rd}}^{\mathrm{shelf}} + F_{\mathrm{mix,40Ar}}^{\mathrm{shelf}} - F_{\mathrm{as,40Ar}}^{\mathrm{atm\text{-}shelf}} \tag{A.11}$$
$$\frac{dR_{\mathrm{40K}}^{\mathrm{shelf}}}{dt} = F_{\mathrm{mix,40K}}^{\mathrm{shelf}} - F_{\mathrm{rd}}^i + F_{\mathrm{w,40K}} \tag{A.12}$$
$$\frac{dR_{\mathrm{K}}^{\mathrm{shelf}}}{dt} = F_{\mathrm{mix,K}}^i + F_{\mathrm{w,K}} \tag{A.13}$$
$$\frac{dR_{\mathrm{PO4}}^{\mathrm{shelf}}}{dt} = F_{\mathrm{mix,PO4}}^{\mathrm{shelf}} - F_{\mathrm{ExT}}^{\mathrm{shelf}} + F_{\mathrm{remin,PO4}}^{\mathrm{shelf}} + F_{\mathrm{w,PO4}} - F_{\mathrm{NO3}}^{\mathrm{shelf}} \tag{A.14}$$
$$\frac{dR_{\mathrm{NO3}}^{\mathrm{shelf}}}{dt} = F_{\mathrm{mix,NO3}}^{\mathrm{shelf}} - F_{\mathrm{out,NO3}}^{\mathrm{shelf}} + F_{\mathrm{nit}}^{\mathrm{shelf}} - F_{\mathrm{den}}^{\mathrm{shelf}} + F_{\mathrm{remin,NO3}}^{\mathrm{shelf}} - F_{\mathrm{NO3}}^{\mathrm{shelf}} \tag{A.15}$$
$$\frac{dR_{\mathrm{NH4}}^{\mathrm{shelf}}}{dt} = F_{\mathrm{mix,NH4}}^{\mathrm{shelf}} - F_{\mathrm{out,NH4}}^{\mathrm{shelf}} - F_{\mathrm{nit}}^{\mathrm{shelf}} + F_{\mathrm{remin,NH4}}^{\mathrm{shelf}} + F_{\mathrm{w,NH4}} - F_{\mathrm{seddif}}^{\mathrm{shelf}} \tag{A.16}$$
$$\frac{dR_{\mathrm{N2}}^{\mathrm{shelf}}}{dt} = F_{\mathrm{mix,N2}}^{\mathrm{shelf}} - F_{\mathrm{out,N2}}^{\mathrm{shelf}} + F_{\mathrm{den}}^{\mathrm{shelf}} \tag{A.17}$$

Deep ocean

$$\frac{dR^{\text{deep}}_{\text{40Ar}}}{dt} = F^{\text{deep}}_{\text{mix,40Ar}} + F^{\text{deep}}_{\text{rd}} - F^{\text{deep}}_{\text{hydro,40Ar}} + F_{\text{ogmor,40Ar}} \quad \text{(A.18)}$$

$$\frac{dR^{\text{deep}}_{\text{36Ar}}}{dt} = F^{\text{deep}}_{\text{mix,36Ar}} - F^{\text{deep}}_{\text{hydro,36Ar}} + F_{\text{ogmor,36Ar}} \quad \text{(A.19)}$$

$$\frac{dR^{\text{deep}}_{\text{40K}}}{dt} = F^{\text{deep}}_{\text{mix,40K}} - F^{\text{deep}}_{\text{rd}} - F_{\text{hydro,40K}} + F_{\text{ogmor,40K}} \quad \text{(A.20)}$$

$$\frac{dR^{\text{deep}}_{\text{K}}}{dt} = F^{\text{deep}}_{\text{mix,K}} - F_{\text{hydro,K}} + F_{\text{ogmor,K}} \quad \text{(A.21)}$$

$$\frac{dR^{\text{deep}}_{\text{PO4}}}{dt} = F^{\text{deep}}_{\text{mix,PO4}} + F^{\text{deep}}_{\text{remin,PO4}} - F_{\text{hydro,PO4}} + F_{\text{ogmor,PO4}} \quad \text{(A.22)}$$

$$\frac{dR^{\text{deep}}_{\text{NO3}}}{dt} = F^{\text{deep}}_{\text{mix,NO3}} + F^{\text{deep}}_{\text{remin,NO3}} + F^{\text{deep}}_{\text{nit}} - F^{\text{deep}}_{\text{den}} - F^{\text{deep}}_{\text{hydro,NO3}} \quad \text{(A.23)}$$

$$\frac{dR^{\text{deep}}_{\text{NH4}}}{dt} = F^{\text{deep}}_{\text{mix,NH4}} - F^{\text{deep}}_{\text{nit}} + F^{\text{deep}}_{\text{remin,NH4}} - F^{\text{deep}}_{\text{seddif}} - F^{\text{deep}}_{\text{hydro,NH4}} \quad \text{(A.24)}$$

$$\frac{dR^{\text{deep}}_{\text{N2}}}{dt} = F^{\text{deep}}_{\text{mix,N2}} + F^{\text{deep}}_{\text{den}} + F_{\text{ogmor,N}} \quad \text{(A.25)}$$

Sediments

$$\frac{dR^{i}_{\text{NO3}}}{dt} = F^{i}_{\text{nit}} - F^{i}_{\text{den}} + F^{iii}_{\text{seddif,NO3}} \quad \text{(A.26)}$$

$$\frac{dR^{i}_{\text{NH4}}}{dt} = F^{i}_{\text{remin,NH4}} - F^{i}_{\text{nit}} + F^{iii}_{\text{seddif,NH4}} \quad \text{(A.27)}$$

$$\frac{dR^{i}_{\text{PO4}}}{dt} = F^{i}_{\text{remin,PO4}} + F^{iii}_{\text{seddif}} \quad \text{(A.28)}$$

$$\frac{dR^{ii}_{\text{N}}}{dt} = F^{i}_{\text{bur,NH4}} - F^{ii}_{\text{sub,NH4}} \quad \text{(A.29)}$$

$$\frac{dR^{ii}_{\text{PO4}}}{dt} = F^{i}_{\text{bur,PO4}} - F^{ii}_{\text{sub,PO4}} \quad \text{(A.30)}$$

for i ={reactive shelf sediments, reactive deep sediments}, ii ={shelf sediments, deep sediments}, and iii ={shelf ocean, deep ocean}.

Ocean crust

$$\frac{dR^{i}_{\text{40Ar}}}{dt} = F_{\text{rd}} - F^{i}_{\text{sub,40Ar}} \quad \text{(A.31)}$$

$$\frac{dR^{i}_{\text{40K}}}{dt} = -F_{\text{rd}} - F^{i}_{\text{sub,40K}} \quad \text{(A.32)}$$

$$\frac{dR^{i}_{\text{K}}}{dt} = F_{\text{hydro,K}} - F^{i}_{\text{sub,K}} \quad \text{(A.33)}$$

$$\frac{dR^{i}_{\text{N}}}{dt} = F_{\text{hydro,N}} - F^{i}_{\text{sub,NH4}} \quad \text{(A.34)}$$

$$\frac{dR^{i}_{\text{PO4}}}{dt} = F_{\text{hydro,PO4}} - F^{i}_{\text{sub,PO4}} \quad \text{(A.35)}$$

for i ={ocean crust}.

Continental crust

$$\frac{dR^i_{40\mathrm{Ar}}}{dt} = F^i_{\mathrm{rd}} - F_{\mathrm{w,40Ar}} \quad \text{(A.36)}$$

$$\frac{dR^i_{40\mathrm{K}}}{dt} = -F^i_{\mathrm{rd}} - F_{\mathrm{w,40K}} \quad \text{(A.37)}$$

$$\frac{dR^i_j}{dt} = F_{\mathrm{cg,j}} - F_{\mathrm{w,j}} \quad \text{(A.38)}$$

for i ={continental crust} and j={K, NH_4^+, PO_4^{3-}}.

Mantle

$$\frac{dR^i_{40\mathrm{Ar}}}{dt} = F^i_{\mathrm{rd}} - F_{\mathrm{ogm,40Ar}} + F_{\mathrm{subnet,40Ar}} \quad \text{(A.39)}$$

$$\frac{dR^i_{40\mathrm{K}}}{dt} = -F^i_{\mathrm{rd}} - F_{\mathrm{ogm,40K}} + F_{\mathrm{subnet,40K}} \quad \text{(A.40)}$$

$$\frac{dR^i_j}{dt} = -F_{\mathrm{ogmor},j} + F_{\mathrm{subnet},j} \quad \text{(A.41)}$$

for i ={mantle} and j = {^{36}Ar, N, PO_4^{3-}, and K}.

B: Calculating initial N distribution

We use the following equation from *Libourel et al.* [2003] to calculate the starting amount of N in the atmosphere and mantle for the nominal run:

$$N_{2,\,\mathrm{magma}} = 2.21 \times 10^{-9} \mathrm{pN_2} + fO_2^{-0.75} 2.13 \times 10^{-17} \mathrm{pN_2^{0.5}} \quad \text{(B.1)}$$

where pN_2 is in atmospheres and $N_{2,\,\mathrm{magma}}$ is in mol g^{-1} atm^{-1}. We chose an fO_2 of IW - 2 ($fO_2 = 10^{-11.4}$), where IW is the iron wüstite buffer, which is the expected oxygen fugacity of the magma ocean immediately after core formation [*Wood et al.*, 2006] (Fig. B.1).

Then, for a variety of pN_2 values, we calculate a magma N_2 concentration at fO_2 = IW-2, and multiply this concentration by the mass of the mantle. This assumes the whole mantle equilibrated during the atmosphere during the magma ocean phase.

Finally, we describe the fraction of the total N budget that is in the atmosphere based on the above solubility calculations. This figure ultimately guided our choice for total N budget and starting atmospheric N mass in the nominal run. We chose 4.5 PAN as the total budget, which results in 82% of the total N starting in the atmosphere. The total N budget was chosen so that the nominal run resulted in a 1 PAN modern atmosphere at the end of the model run.

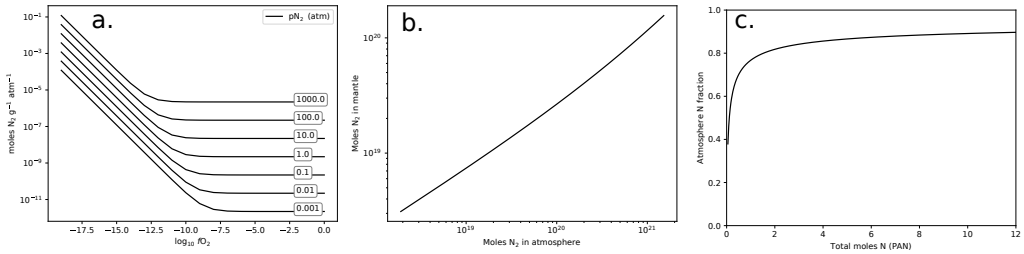

Figure B.1: Nitrogen solubility in basaltic magma used to calculate starting atmospheric N. a.) Basaltic magma N_2 content as a function of oxygen fugacity. Lines are for different pN_2, with pressure in atmospheres shown in boxes. Modified after *Libourel et al.* [2003]. b.) Total mantle and atmospheric N based on the solubility experiments of *Libourel et al.* [2003] at the end of core formation. c.) Atmospheric fraction of N as a function of total N (PAN) for an atmosphere in equilibrium with the mantle at the end of the magma ocean phase. Oxygen fugacity is IW - 2.

C: Argon and potassium model performance checks

We use argon concentration in the atmosphere as a check on the performance of degassing and air-sea gas exchange in the model. The model overestimates the modern day ratio of $^{40}Ar/^{36}Ar$ in the atmosphere by about 1.5 fold (Fig. C.1). It is possible that this slight overestimate is due in part to the model underestimating K concentration in the continental crust (Fig. C.1). Higher K-content in the crust would lead to more ^{40}Ar in the crust, through storage after radioactive decay of ^{40}K, and would then lower the atmospheric Ar-ratio.

While the model output reproduces the K content of the mantle well, it underestimates the continental crust concentration. Weathering is simply proportional to concentration in the model, and does not take into account either differences in weathering due to biologic activity or continental growth over time. Given different amounts of crustal growth over time [e.g., *Dhuime et al.*, 2012], the continents would evolve in their capacity to store K over time. In addition, we do not consider the effects of continental lithospheric roots or cratonic mass, which could serve to store K for long periods during Earth history. Future iterations of the EarthN model should incorporate crustal growth scenarios.

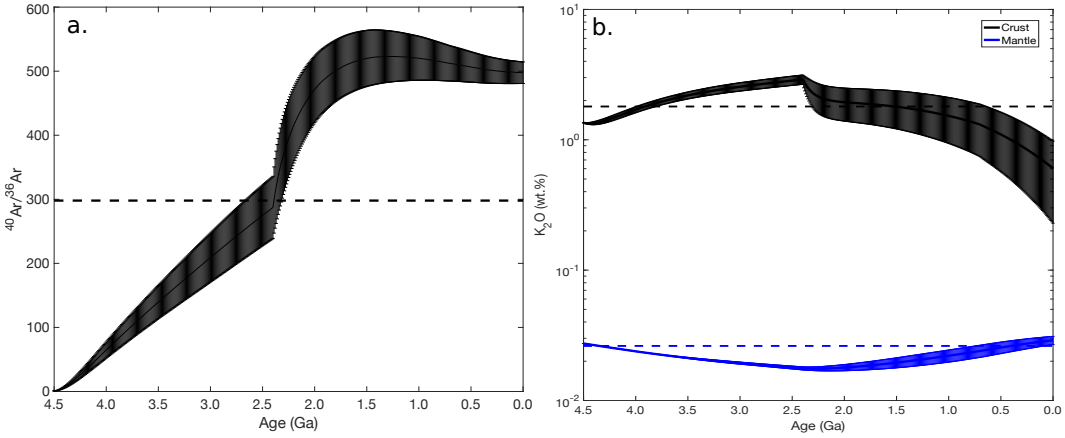

Figure C.1: Atmospheric^{40}Ar/^{36}*Ar* and K concentrations (wt. %K_2O) for continental crust and mantle from Monte Carlo runs. The mean and one standard deviation are shown, and modern values are given as dashed line [*Rudnick and Gao*, 2014; *Arevalo et al.*, 2013].

References

Anbar, A. D., Y. Duan, T. W. Lyons, G. L. Arnold, B. Kendall, R. A. Creaser, A. J. Kaufman, G. W. Gordon, C. Scott, J. Garvin, et al. (2007), A whiff of oxygen before the great oxidation event?, *Science*, *317*(5846), 1903–1906, doi:10.1126/science.1140325.

Arevalo, R., W. F. McDonough, A. Stracke, M. Willbold, T. J. Ireland, and R. J. Walker (2013), Simplified mantle architecture and distribution of radiogenic power, *Geochemistry, Geophysics, Geosystems*, *14*(7), 2265–2285, doi:http://dx.doi.org/10.1002/ggge.20152.

Barry, P., and D. Hilton (2016), Release of subducted sedimentary nitrogen throughout Earth's mantle, *Geochemical Perspectives Letters*, *2*, 148–159.

Bebout, G., and M. Fogel (1992), Nitrogen-isotope compositions of metasedimentary rocks in the Catalina Schist, California: implications for metamorphic devolatilization history, *Geochimica et Cosmochimica Acta*, *56*(7), 2839–2849, doi:http://dx.doi.org/10.1016/0016-7037(92)90363-N.

Bebout, G. E., K. E. Lazzeri, and C. A. Geiger (2015), Pathways for nitrogen cycling in the Earth's crust and upper mantle: A review and new results for microporous beryl and cordierite, *American Mineralogist*, doi:http://dx.doi.org/10.2138/am-2015-5363.

Berner, R. A. (2006), Geological nitrogen cycle and atmospheric N_2 over phanerozoic time, *Geology*, *34*(5), 413–415, doi:http://dx.doi.org/10.1130/G22470.1.

Boyd, S. (2001), Nitrogen in future biosphere studies, *Chemical Geology*, *176*(1), 1–30, doi:http://dx.doi.org/10.1016/S0009-2541(00)00405-8.

Bradley, D. C. (2008), Passive margins through earth history, *Earth-Science Reviews*, *91*(1), 1–26, doi:http://dx.doi.org/10.1016/j.earscirev.2008.08.001.

Bristow, L. A., T. Dalsgaard, L. Tiano, D. B. Mills, A. D. Bertagnolli, J. J. Wright, S. J. Hallam, O. Ulloa, D. E. Canfield, N. P. Revsbech, et al. (2016), Ammonium and nitrite oxidation at nanomolar oxygen concentrations in oxygen minimum zone waters, *Proceedings of the National Academy of Sciences*, *113*(38), 10,601–10,606, doi:http://dx.doi.org/10.1073/pnas.1600359113.

Brounce, M., K. Kelley, and E. Cottrell (2014), Variations in $Fe^{3+}/\Sigma Fe$ of Mariana Arc Basalts and Mantle Wedge fO_2, *Journal of Petrology*, *55*(12), 2513–2536.

Buick, R. (2008), When did oxygenic photosynthesis evolve?, *Philosophical Transactions of the Royal Society of London B: Biological Sciences*, *363*(1504), 2731–2743.

Busigny, V., P. Cartigny, and P. Philippot (2011), Nitrogen isotopes in ophiolitic metagabbros: A re-evaluation of modern nitrogen fluxes in subduction zones and implication for the early earth atmosphere, *Geochimica et Cosmochimica Acta*, *75*, 7502–7521, doi:http://dx.doi.org/10.1016/j.gca.2011.09.049.

Canil, D. (2002), Vanadium in peridotites, mantle redox and tectonic environments: Archean to present, *Earth and Planetary Science Letters*, *195*(1), 75–90, doi:http://dx.doi.org/10.1016/S0012-821X(01)00582-9.

Catling, D. C., and J. F. Kasting (2017), *Atmospheric evolution on inhabited and lifeless worlds*, Cambridge University Press.

Condie, K. C. (2013), *Plate tectonics & crustal evolution*, Elsevier.

Crowe, S. A., D. E. Canfield, A. Mucci, B. Sundby, and R. Maranger (2012), Anammox, denitrification and fixed-nitrogen removal in sediments from the lower st. lawrence estuary, *Biogeosciences*, *9*(11), 4309–4321.

Dalsgaard, T., F. J. Stewart, B. Thamdrup, L. D. Brabandere, N. P. Revsbech, O. Ulloa, D. E. Canfield, and E. F. DeLong (2014), Oxygen at nanomolar levels reversibly suppresses process rates and gene expression in anammox and denitrification in the oygen minimum zone off Northern Chile, *mBio*, *5*, e01,966–14.

Delwiche, C. (1977), Energy relations in the global nitrogen cycle, *Ambio*, pp. 106–111.

Dhuime, B., C. Hawkesworth, P. Cawood, and C. Stoery (2012), A change in the geodynamics of continental growth 3 billion years ago, *Science*, *335*, 1334–1336, doi:

http://dx.doi.org/10.1126/science.1216066.

Elderfield, H., and A. Schultz (1996), Mid-ocean ridge hydrothermal fluxes and the chemical composition of the ocean, *Annual Review of Earth and Planetary Sciences*, *24*(1), 191–224.

Elkins, L., T. Fischer, D. Hilton, Z. Sharp, S. McKnight, and J. Walker (2006), Tracing nitrogen in volcanic and geothermal volatiles from the Nicaraguan volcanic front, *Geochimica et Cosmochimica Acta*, *70*(20), 5215–5235, doi:http://dx.doi.org/10.1016/j.gca.2006.07.024.

Evrard, V., R. N. Glud, and P. L. Cook (2013), The kinetics of denitrification in permeable sediments, *Biogeochemistry*, *113*, 563–572, doi:10.1007/s10533-012-9789-x.

Farquhar, J., Jhar, H. Bao, and M. Thiemens (2000), Atmospheric influence of Earth's earliest sulfur cycle, *Science*, *289*, 756–758, doi:http://dx.doi.org/10.1126/science.289.5480.756.

Fennel, K., M. Follows, and P. G. Falkowski (2005), The co-evolution of the nitrogen, carbon and oxygen cycles in the proterozoic ocean, *American Journal of Science*, *305*(6-8), 526–545, doi:http://dx.doi.org/10.2475/ajs.305.6-8.526.

Fischer, T., D. Hilton, M. Zimmer, A. Shaw, Z. Sharp, and J. Walker (2002), Subduction and recycling of nitrogen along the Central American margin, *Science*, *297*(5584), 1154–1157, doi:http://dx.doi.org/10.1126/science.1073995.

Frost, D., and C. McCammon (2008), The redox state of Earth's mantle, *Annual Review of Earth and Planetary Sciences*, *36*, 389–420, doi:http://dx.doi.org/10.1146/annurev.earth.36.031207.124322.

Garcia, H., R. Locarnini, T. Boyer, J. Antonov, O. Baranova, M. Zweng, J. Reagan, and D. Johnson (2014), Dissolved inorganic nutrients (phosphate, nitrate, silicate), *World Ocean Atlas*, *4*, 25.

German, C., and W. Seyfried (2014), Hydrothermal processes., *Treatise on Geochemistry*, 191–233.

Goering, J. J. (1985), Marine denitrification, in *Denitrification in the nitrogen cycle*, pp. 191–224, Springer.

Goldblatt, C., T. Lenton, and A. Watson (2006), Bistability of atmospheric oxygen and the Great Oxidation, *Nature*, *443*(7112), 683–686.

Goldblatt, C., M. Claire, T. Lenton, A. Matthews, A. Watson, and K. Zahnle (2009), Nitrogen-enhanced greenhouse warming on early Earth, *Nature Geoscience*, *2*(12), 891–

889 896, doi:http://dx.doi.org/10.1038/ngeo692.

890 Gruber, N. (2008), The marine nitrogen cycle: overview and challenges, *Nitrogen in the*
891 *marine environment*, *2*, 1–50.

892 Gruber, N., and J. Galloway (2008), An Earth-system perspective of the global nitrogen
893 cycle, *Nature*, *451*(7176), 293–296.

894 Halama, R., G. Bebout, T. John, and M. Scambelluri (2014), Nitrogen recycling in sub-
895 ducted mantle rocks and implications for the global nitrogen cycle, *International Jour-*
896 *nal of Earth Sciences*, pp. 1–19, doi:http://dx.doi.org/10.1007/s00531-012-0782-3.

897 Halliday, A. N. (2013), The origins of volatiles in the terrestrial planets, *Geochimica et*
898 *Cosmochimica Acta*, *105*, 146–171, doi:http://dx.doi.org/10.1016/j.gca.2012.11.015.

899 Haynes, W., T. Bruno, and D. Lide (Eds.) (2014), *CRC Handbook of Chemistry and*
900 *Physics 95*, CRC Press.

901 Hofmann, H., K. Grey, A. Hickman, and R. Thorpe (1999), Origin of 3.45 Ga coniform
902 stromatolites in Warrawoona group, Western Australia, *Geological Society of America*
903 *Bulletin*, *111*(8), 1256–1262.

904 Houlton, B., S. Morford, and R. Dahlgren (2018), Convergent evidence for widespread
905 rock nitrogen sources in Earth's surface environment, *Science*, *360*(6384), 58–62.

906 Johnson, B. W., and C. Goldblatt (2015), The nitrogen budget of earth, *Earth Science Re-*
907 *views*, *148*, 150–173, doi:http://dx.doi.org/10.1016/j.earscirev.2015.05.006.

908 Johnson, B. W., and C. Goldblatt (2017), A secular increase in continental crust nitrogen
909 during the Precambrian, *Geochemical Perspectives Letters*, *4*, 24–28.

910 Kelley, K. A., and E. Cottrell (2012), The influence of magmatic differentiation on the
911 oxidation state of Fe in a basaltic arc magma, *Earth and Planetary Science Letters*, *329*,
912 109–121.

913 Klingler, J., R. Mancinelli, and M. White (1989), Biological nitrogen fixation under pri-
914 mordial martian partial pressures of dinitrogen, *Advances in Space Research*, *9*(6), 173–
915 176, doi:http://dx.doi.org/10.1016/0273-1177(89)90225-1.

916 Korenaga, J. (2010), Scaling of plate tectonic convection with pseudoplastic rheology,
917 *Journal of Geophysical Research: Solid Earth (1978–2012)*, *115*(B11), doi:http://dx.doi.
918 org/10.1029/2010JB007670.

919 Laneuville, M., M. Kameya, and H. J. Cleaves (2018), Earth Without Life: A Systems
920 Model of a Global Abiotic Nitrogen Cycle, *Astrobiology*.

Li, L., G. Bebout, and B. Idleman (2007), Nitrogen concentration and δ^{15}N of altered oceanic crust obtained on ODP Legs 129 and 185: Insights into alteration-related nitrogen enrichment and the nitrogen subduction budget, *Geochimica et Cosmochimica Acta*, *71*, 2344–2360, doi:http://dx.doi.org/10.1016/j.gca.2007.02.001.

Li, Y., and H. Keppler (2014), Nitrogen speciation in mantle and crustal fluids, *Geochimica et Cosmochimica Acta*, *129*, 13–32, doi:http://dx.doi.org/10.1016/j.gca.2013.12.031.

Li, Y., R. Huang, M. Wiedenbeck, and H. Keppler (2015), Nitrogen distribution between aqueous fluids and silicate melts, *Earth and Planetary Science Letters*, *411*, 218–228, doi:http://dx.doi.org/10.1016/j.epsl.2014.11.050.

Li, Y., M. Wiedenbeck, S. Shcheka, and H. Keppler (2013), Nitrogen solubility in upper mantle minerals, *Earth and Planetary Science Letters*, *377*, 311–323, doi:http://dx.doi.org/10.1016/j.epsl.2013.07.013.

Li, Y., B. Marty, S. Shcheka, L. Zimmermann, and H. Keppler (2016), Nitrogen isotope fractionation during terrestrial core-mantle separation, *Geochemical Perspectives Letters*, *2*(2), 138–147, doi:10.7185/geochemlet.1614.

Libourel, G., B. Marty, and F. Humbert (2003), Nitrogen solubility in basaltic melt. Part I. Effect of oxygen fugacity, *Geochimica et Cosmochimica Acta*, *67*(21), 4123–4135, doi:http://dx.doi.org/10.1016/S0016-7037(03)00259-X.

Liss, P., and P. Slater (1974), Flux of Gases across the Air-Sea Interface, *Nature*, *247*, 181–184.

Lyons, T. W., C. T. Reinhard, and N. J. Planavsky (2014), The rise of oxygen in Earth's early ocean and atmosphere, *Nature*, *506*(7488), 307–315.

Mallik, A., Y. Li, and M. Wiedenbeck (2018), Nitrogen evolution within the Earth's atmosphere–mantle system assessed by recycling in subduction zones, *Earth and Planetary Science Letters*, *482*, 556–566.

Marty, B. (2012), The origins and concentrations of water, carbon, nitrogen and noble gases on Earth, *Earth and Planetary Science Letters*, *313*, 56–66, doi:http://dx.doi.org/10.1016/j.epsl.2011.10.040.

Marty, B., L. Zimmermann, M. Pujol, R. Burgess, and P. Philippot (2013), Nitrogen isotopic composition and density of the Archean atmosphere., *Science*, *342*, 101–104, doi:http://dx.doi.org/10.1126/science.1240971.

Mikhail, S., and D. Howell (2016), Outlooks in Earth and Planetary Materials: Chemistry and Mineralogy of Earth's Mantle: A petrological assessment of diamond as a recorder

of the mantle nitrogen cycle, *American Mineralogist*, *101*(4), 780–787.

Mikhail, S., and D. A. Sverjensky (2014), Nitrogen speciation in upper mantle fluids and the origin of Earth's nitrogen-rich atmosphere, *Nature Geoscience*, *7*, 816–819, doi:http://dx.doi.org/10.1038/ngeo2271.

Mitchell, E. C., T. P. Fischer, D. R. Hilton, E. H. Hauri, A. M. Shaw, J. M. de Moor, Z. D. Sharp, and K. Kazahaya (2010), Nitrogen sources and recycling at subduction zones: Insights from the Izu-Bonin-Mariana arc, *Geochemistry, Geophysics, Geosystems*, *11*(2), doi:http://dx.doi.org/10.1029/2009GC002783.

Nance, R. D., and J. B. Murphy (2013), Origins of the supercontinent cycle, *Geoscience Frontiers*, *4*(4), 439–448.

Navarro-González, R., C. P. McKay, and D. N. Mvondo (2001), A possible nitrogen crisis for Archaean life due to reduced nitrogen fixation by lightning, *Nature*, *412*(6842), 61.

Nishizawa, M., Y. Sano, Y. Ueno, and S. Maruyama (2007), Speciation and isotope ratios of nitrogen in fluid inclusions from seafloor hydrothermal deposits at 3.5 Ga, *Earth and Planetary Science Letters*, *254*(3), 332–344, doi:http://dx.doi.org/10.1016/j.epsl.2006.11.044.

Padhi, C. M., J. Korenaga, and M. Ozima (2012), Thermal evolution of Earth with xenon degassing: a self-consistent approach, *Earth and Planetary Science Letters*, *341*, 1–9, doi:http://dx.doi.org/10.1016/j.epsl.2012.06.013.

Planavsky, N. J., C. T. Reinhard, X. Wang, D. Thomson, P. McGoldrick, R. H. Rainbird, T. Johnson, W. W. Fischer, and T. W. Lyons (2014), Low Mid-Proterozoic atmospheric oxygen levels and the delayed rise of animals, *Science*, *346*(6209), 635–638.

Reinhard, C. T., N. J. Planavsky, S. L. Olson, T. W. Lyons, and D. H. Erwin (2016), Earth's oxygen cycle and the evolution of animal life, *Proceedings of the National Academy of Sciences*, p. 201521544.

Rudnick, R., and S. Gao (2014), Composition of the Continental Crust, *Treatise on Geochemistry*, *4*, 1–69, doi:http://dx.doi.org/10.1016/S0016-7037(00)00393-8.

Sander, R. (1999), Compilation of Henry's law constants for inorganic and organic species of potential importance in environmental chemistry, Max-Planck Institute of Chemistry, Air Chemistry Department Mainz, Germany, doi:http://www.mpch-mainz.mpg.de/~sander/res/henry.html.

Sandu, C., A. Lenardic, and P. McGovern (2011), The effects of deep water cycling on planetary thermal evolution, *Journal of Geophysical Research*, *116*, 1–15, doi:http://dx.

987 doi.org/10.1029/2011JB008405.

988 Sleep, N. H., and B. F. Windley (1982), Archean plate tectonics: constraints and infer-
989 ences, *The Journal of Geology*, *90*(4), 363–379.

990 Smith, E. M., M. G. Kopylova, and W. Peck (2014), Implications of metallic iron for dia-
991 monds and nitrogen in the sublithospheric mantle, *Canadian Journal of Earth Sciences*,
992 *51*(5), 510–516, doi:http://dx.doi.org/10.1139/cjes-2013-0218.

993 Som, S. M., D. C. Catling, J. P. Harnmeijer, P. M. Polivka, and R. Buick (2012), Air den-
994 sity 2.7 billion years ago limited to less than twice modern levels by fossil raindrop im-
995 prints, *Nature*, *484*(7394), 359–362, doi:http://dx.doi.org/10.1038/nature10890.

996 Som, S. M., R. Buick, J. W. Hagadorn, T. S. Blake, J. M. Perreault, J. P. Harnmeijer, and
997 D. C. Catling (2016), Earth's air pressure 2.7 billion years ago constrained to less than
998 half of modern levels, *Nature Geoscience*, *9*, 448–451.

999 Stüeken, E., R. Buick, B. M. Guy, and M. C. Koehler (2015), Isotopic evidence for bi-
1000 ological nitrogen fixation by molybdenum-nitrogenase from 3.2 Gyr, *Nature*, doi:
1001 http://dx.doi.org/10.1038/nature14180.

1002 Stüeken, E., M. Kipp, M. Koehler, E. Schwieterman, B. W. Johnson, and R. Buick (2016),
1003 Modeling pN2 through geologic time: Implications for atmospheric biosignatures, *As-*
1004 *trobiology*, *16*(12), 949–963.

1005 Tolstikhin, I., and B. Marty (1998), The evolution of terrestrial volatiles: a view from he-
1006 lium, neon, argon and nitrogen isotope modelling, *Chemical Geology*, *147*(1-2), 27–52.

1007 Van Hunen, J., and J.-F. Moyen (2012), Archean subduction: fact or fiction?, *Annual Re-*
1008 *view of Earth and Planetary Sciences*, *40*, 195–219.

1009 Vitousek, P. M., D. N. Menge, S. C. Reed, and C. C. Cleveland (2013), Biological ni-
1010 trogen fixation: rates, patterns and ecological controls in terrestrial ecosystems, *Philo-*
1011 *sophical Transactions of the Royal Society of London B: Biological Sciences*, *368*(1621),
1012 20130,119.

1013 Watenphul, A., B. Wunder, and W. Heinrich (2009), High-pressure ammonium-bearing sil-
1014 icates: Implications for nitrogen and hydrogen storage in the Earth's mantle, *American*
1015 *Mineralogist*, *94*(2-3), 283–292, doi:http://dx.doi.org/10.2138/am.2009.2995.

1016 Watenphul, A., B. Wunder, R. Wirth, and W. Heinrich (2010), Ammonium-bearing
1017 clinopyroxene: A potential nitrogen reservoir in the Earth's mantle, *Chemical Geology*,
1018 *270*(1), 240–248, doi:http://dx.doi.org/10.1016/j.chemgeo.2009.12.003.

1019 Winter, J. D. (2001), *An introduction to igneous and metamorphic petrology*, vol. 697,
1020 Prentice Hall New Jersey.

1021 Wood, B. J., M. J. Walter, and J. Wade (2006), Accretion of the Earth and segregation of
1022 its core, *Nature*, *441*(7095), 825–833.

1023 Wordsworth, R., and R. Pierrehumbert (2013), Hydrogen-nitrogen greenhouse warming in
1024 earth's early atmosphere, *Science*, *339*(6115), 64–67.

1025 Yoshioka, T., M. Wiedenbeck, S. Shcheka, and H. Keppler (2018), Nitrogen solubility in
1026 the deep mantle and the origin of Earth's primordial nitrogen budget, *Earth and Plane-*
1027 *tary Science Letters*, *488*, 134–143.

1028 Zelenski, M., Y. A. Taran, E. Dubinina, E. Polyntseva, et al. (2012), Sources of volatiles
1029 for a subduction zone volcano: Mutnovsky volcano, Kamchatka, *Geochemistry Interna-*
1030 *tional*, *50*(6), 502–521.

1031 Zerkle, A., and S. Mikhail (2017), The geobiological nitrogen cycle: From microbes to the
1032 mantle, *Geobiology*, *15*, 343–352.

1033 Zhang, S., X. Wang, H. Wang, C. J. Bjerrum, E. U. Hammarlund, M. M. Costa, J. N.
1034 Connelly, B. Zhang, J. Su, and D. E. Canfield (2016), Sufficient oxygen for animal
1035 respiration 1,400 million years ago, *Proceedings of the National Academy of Sciences*,
1036 *113*(7), 1731–1736.

1037 Zhang, Y., and A. Zindler (1993), Distribution and evolution of carbon and nitrogen in
1038 Earth, *Earth and Planetary Science Letters*, *117*(3), 331–345.